NEUTRON POLARIZATIONS FROM (d,n) REACTIONS ON ^{11}B, ^{24}Mg, ^{28}Si, AND ^{40}Ca

by

John Taylor

Department of Physics
Duke University

Date: ____________________

Approved:

Richard L Walter
R. L. Walter, Supervisor

____

____

____

____

A dissertation submitted in partial fulfillment of the requirements for the degree of Doctor of Philosophy in the Department of Physics in the Graduate School of Arts and Sciences of Duke University

1971

Physics Library
T 24 J
1971

ABSTRACT

(Physics)

NEUTRON POLARIZATIONS FROM (d,n) REACTIONS ON ^{11}B, ^{24}Mg, ^{28}Si, AND ^{40}Ca

by

John Taylor

Department of Physics
Duke University

Date: _____

Approved:

Richard L Walter
R. L. Walter, Supervisor

_____

_____

_____

_____

An abstract of a dissertation submitted in partial fulfillment of the requirements for the degree of Doctor of Philosophy in the Department of Physics in the Graduate School of Arts and Sciences of Duke University

1971

ACKNOWLEDGMENTS

I would like to express my deep appreciation to my advisor, Dr. Richard L. Walter, for his continued guidance and support throughout the course of this project. I am also deeply indebted to Dr. Thomas Stammbach for his generous help in conducting the experiments and for many stimulating and helpful discussions concerning the data.

Special thanks are due Mr. George Spalek, who designed the polarimeter used in most of these measurements and who gave generously of his time during the collection of the data. Mr. Robert Hardekopf undertook the measurement of $^{11}B(d,d)$ elastic cross section in order to facilitate the analysis of the $^{11}B(d,n)$ data. For this and for his help in several other phases of this work I am deeply indebted. I would also like to thank Mr. Thomas Rhea for his help in taking some of the data and Mr. Steve Chevront for his help in analyzing part of the $^{28}Si(d,n)$ data. I am grateful to Dr. James Joyce for many helpful discussions and for reading the manuscript. Thanks are extended to Dr. W. Thompson for several enlightening conversations concerning the DWBA.

I wish to thank Dr. N. R. Roberson for his help with the computer interface and Dr. R. V. Poore for his help with the data acquisition software. A debt of gratitude is owed Mr. S. E. Edwards for his excellent maintenance of the often balky computer hardware. I would also like to thank Mr. R. Rummel and Mr. M. Smith for their help with the Van de Graaffs. Mrs. Joseph Bailey prepared the drawings and her work is greatly appreciated.

I am deeply indebted to my parents for their continued encouragement and to my wife, Martha, for her considerable encouragement and patience throughout the course of this work.

This work was supported in part by the U. S. Atomic Energy Commission.

J. T.

CONTENTS

LIST OF FIGURES

LIST OF TABLES

NEUTRON POLARIZATIONS FROM (d,n) REACTIONS ON ^{11}B, ^{24}Mg, ^{28}Si, AND ^{40}Ca

Chapter I

INTRODUCTION

One-particle stripping reactions have been demonstrated to be quite useful in nuclear spectroscopy. The cross section angular distributions have long been used to determine the orbital angular momentum transfer values of the stripped nucleon. On the other hand, the polarization angular distributions are useful in determining the total angular momentum transfer. The extraction of this information usually requires the use of one of the direct reaction models, the best known of which is the Distorted Wave Born Approximation (DWBA). However the DWBA results for light nuclei have been inconsistent and in many cases poor, particularly in the description of the polarization data. In no case is the agreement with the data as good as for some of the intermediate weight nuclei (see for example the $^{52}Cr(d,p)$ analysis of Bjorkholm et al.[1]). It is important to know if these inconsistencies are due to an inadequate model or if the model is simply being applied inappropriately. It is felt that polarization data provides information to which the reaction models are particularly sensitive, and this increases the

importance of this type of data.

There are many possible reasons for the inconsistent results of DWBA calculations on light nuclei. Compound nucleus contributions to the reaction mechanism are sometimes large and fluctuating, and the separation of the competing reaction modes is difficult. Moreover, many of the (d,n) experiments have been done at low energies where these problems are often particularly severe.

Another basic question concerns the generation of the wave functions for the relative motion of the two particles in each channel, which are used to calculate the DWBA transition amplitude. The DWBA model for the reaction A(a,b)B assumes that the wave functions describing the relative motion of a and A and the motion of b and B can be approximated by wave functions generated from an optical model analysis of the appropriate elastic scattering data. The problem with this approach is that the wave functions are not necessarily determined in the nuclear interior, and this region greatly influences the reaction cross sections and polarizations. It is not always clear what forms of optical model potentials should be used to describe the scattering data on light nuclei. This is especially true for the imaginary terms, for which a wide variety of shapes are currently in use. The importance of the tensor force is still relatively undetermined, especially for light nuclei. The magnitude of the spin-orbit force is open to question although its importance has been adequately demonstrated. Polarization measurements should help resolve some of the difficulties and should

also be quite useful in comparing the different reaction models.

This thesis describes neutron polarization measurements from (d,n) reactions on several light nuclei using unpolarized incident beams. Included are reactions with ℓ-transfer values of 0, 1, 2, and 3. The reactions studied were the $^{11}B(d,n_0)$, $^{11}B(d,n_1)$, $^{24}Mg(d,n_0)$, $^{24}Mg(d,n_1)$, $^{28}Si(d,n_0)$, $^{28}Si(d,n_1)$, and $^{40}Ca(d,n_0)$ reactions. Of these reactions only the $^{11}B(d,n_1)$ reaction involves the possible mixing of different orbital angular momentum transfers, as the rest of the reactions have the total angular momentum of either the target or the residual nucleus equal to zero. The analysis is therefore considerably simplified. The ^{11}B measurements were performed with beams from the tandem Van de Graaff. The other reactions were studied earlier using the 4 MeV Van de Graaff, partly as a survey of possible tandem measurements and partly to extend to heavier nuclei a previous polarization study. From these experiments $^{28}Si(d,n)$ was selected for a second tandem measurement at 8.1 MeV.

Chapter II describes some of the techniques involved in neutron polarization measurements and the methods used to extract the polarization values from the raw data. Chapters III and VI describe successively the $^{11}B(d,n)$, $^{28}Si(d,n)$, $^{24}Mg(d,n)$, and $^{40}Ca(d,n)$ reactions. Chapter VII states some of the conclusions of the present work. Appendix A is used to detail one of the more important computer codes used in the data analysis of polarization experiments at our laboratory, and Appendix B lists the $^{11}B(d,d)$ elastic scattering data of Hardekopf et al.[20] which was used in the ^{11}B optical model analysis and which has not previously been published.

Chapter II

EXPERIMENTAL MATTERS AND DATA REDUCTION

A. Experimental Setup and Data Acquisition

The polarimeter and target area setup used in these measurements is shown schematically in Fig. 1. A gaseous ^{4}He scintillator similar to the one described by Morgan and Walter[2] was used as a central scatterer. Two side detectors were placed above and below the helium cell at equal scattering angles θ_2. A solenoid was used to precess the neutron spin direction about the neutron beam axis, i.e., the solenoid axis. The roles of the two side detectors could be interchanged by precessing the beam polarization from $\phi = 90^\circ$ to $\phi = -90^\circ$. This was done by simply reversing the current flowing through the solenoid. The side detectors were either plastic or liquid organic scintillators, and like the helium cell, were connected by Lucite light pipes to RCA-6810 photomultipliers.

The helium cell was prepared in a manner essentially the same as that described by Morgan and Walter.[2] A thinner MgO coating was used on the later cells and was found to give nearly equivalent results. Thin strips

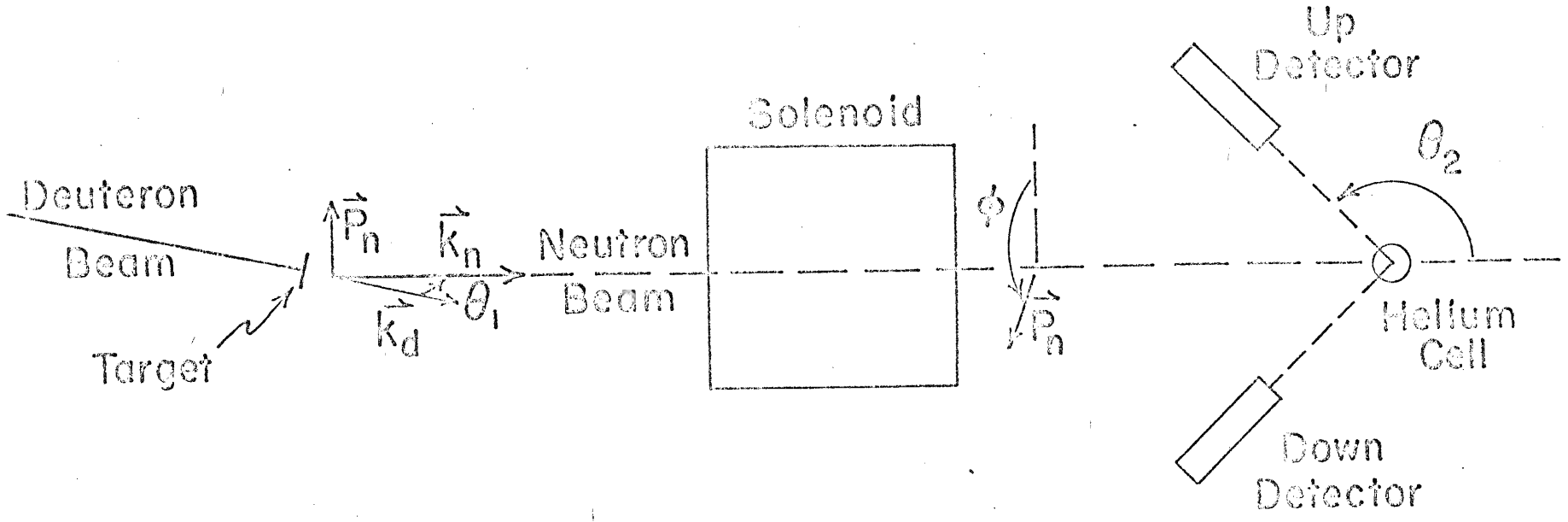

Figure 1. Schematic Diagram of Target Area Setup and Polarimeter.

of Mg ribbon were burned under the cell until the deposited MgO coating was completely opaque. The wavelength shifter p-p' diphenylstilbene was then deposited on the MgO in one evaporation. In particular, 100 mg of the diphenylstilbene was evaporated from a 1 cm diameter boat placed 1 cm inside the cell. The coating on the glass window was obtained by evaporating 15 mg of the wavelength shifter from a distance of 10 cm. After outgassing the cell at a high vacuum for several days it was filled to 140 atm. with a mixture of 5% Xe and 95% He. The cells usually had very high resolution for only a few days but were usable for some of the experiments up to three months after coating. (It is suggested that they might be kept in the optimum condition if they are stored at dry ice temperatures instead of at room temperatures, but this procedure has not been tried.) The cells could be refilled three or four times before they had to be recoated due to deterioration of the wall coating.

The recoil alpha-particle pulses in the helium cell were recorded in coincidence with signals from the side detectors. Figure 2 shows a simplified diagram of electronics used. A slow signal from the eleventh dynode of the center detector was analyzed by an analog-to-digital converter (ADC) yielding a measurement of the recoil energy. Fast signals from the anodes of the photomultiplier tubes triggered fast discriminators to produce fast logic signals which were in turn fed into the appropriate "AND" units with resolving times of less than 10 ns. A later setup used a strobe coincidence unit instead of separate "AND" units. The resultant coincidence gate was

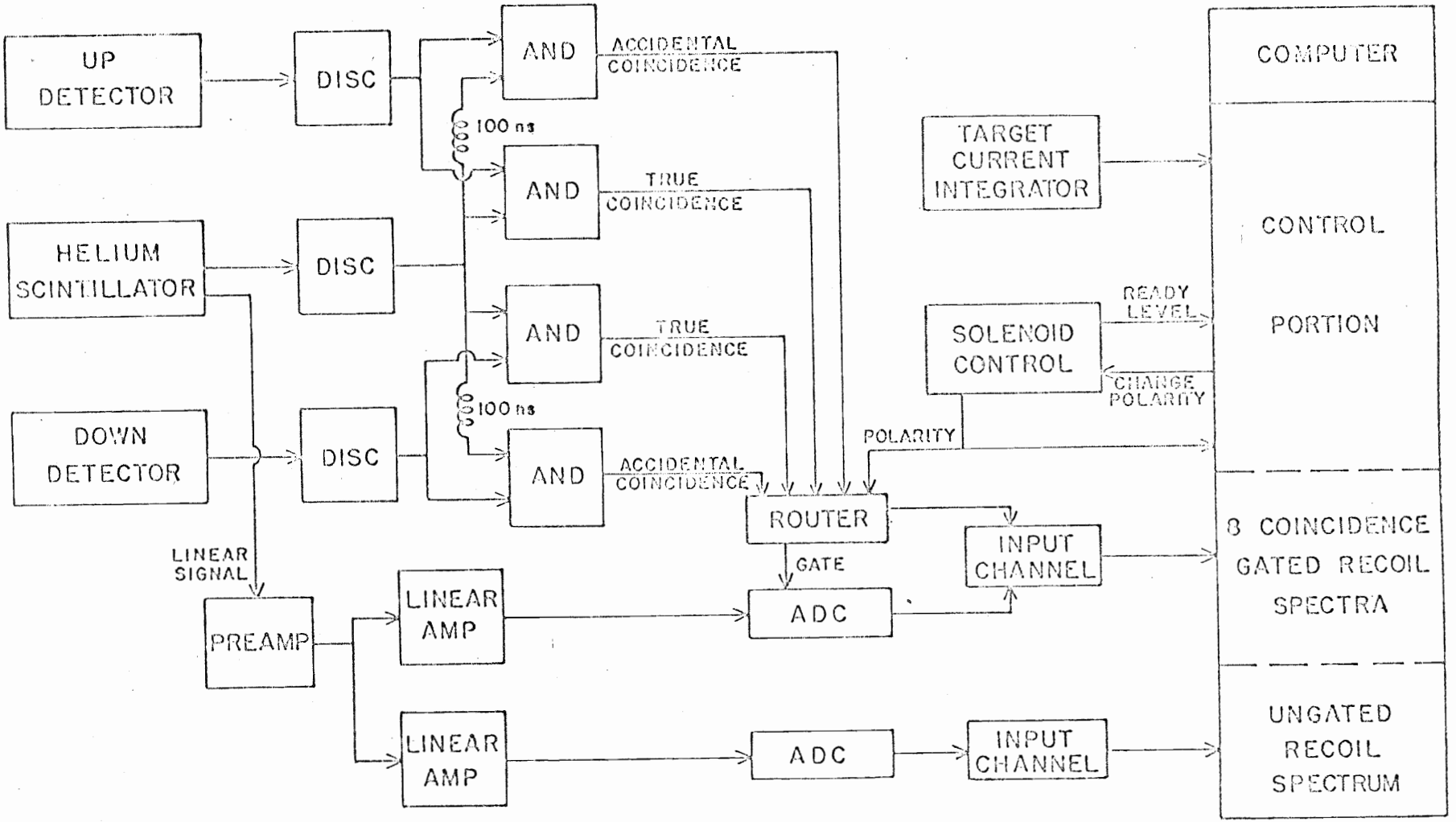

Figure 2. Block Diagram of Fast Coincidence Circuitry and Linear Signal Measurement.

encoded by a router and combined into one 10 bit data word with the corresponding pulse height measurement from the ADC. This word was sent through an input channel to the computer in a high interrupt level. The computer stored the event in one of eight 128-channel spectra corresponding to its combination of side detector, solenoid current direction, and "true" or "accidental" coincidence. The computer code handling the data storage will be discussed more fully below. Simultaneous accumulation of accidental coincidences along with the true coincidences enabled accurate accidental-coincidence background subtraction, but care had to be taken to insure that the pulse length of the direct and delayed signals at the inputs of the "AND" units were identical. The 100 ns delays were sufficient to insure that any coincidence between the delayed center signal and a side detector signal was completely accidental.

A multipurpose computer code was written to handle the experiment using the TUNL time-sharing computer system.[3] The coincidence data were sent to the computer on a high interrupt level. The router encoded the data by setting the three high order bits and the interrupt level routine added a base address in order to calculate the location to be incremented. An ungated helium recoil spectrum was accumulated simultaneously on a lower interrupt level. Each of the eight coincidence spectra, a spectrum consisting of the sum of the foregrounds minus the sum of the backgrounds, and the ungated recoil spectrum could be displayed on a cathode ray tube. The spectra were retained after each measurement so that a

preliminary analysis could be made simultaneously with data accumulation for the next point. In addition, any previous run could be read back from magnetic tape.

The on-line analysis usually consisted of simply calculating the asymmetry of counts in the side detectors between two channels or a series of asymmetries in a predetermined order. For example, calculations could be made holding the upper channel fixed and stepping the lower channel number. Such calculations are useful in extracting asymmetries for two overlapping groups. Asymmetry values determined in this way usually agreed quite well with values obtained later by fitting the spectra with Gaussian line shapes. In addition, line printer plots could be made of any of the eight coincidence spectra, the summed spectrum, and the recoil spectrum. This early analysis proved to be quite valuable in determining the course of the experiment. Data points which needed to be rechecked and others which needed to be measured for the first time were apparent while there was still accelerator time to perform the measurements.

A control section was written for the computer code to sequence the acquisition for a data point and thereby relieve the experimenter from having to pay constant attention to trivial tasks. Short runs of equal charge were taken with the solenoid sequence "cw", "ccw", "ccw", "cw", where "cw" stands for clockwise and "ccw" for counter-clockwise spin precession. The solenoid control circuit was designed by R. S. Thomason[4] and D. Sukis.[5] At the end of each short run, the computer switched the polarity if necessary,

typed the number of coincidence counts from each side detector, and waited for the solenoid current to assume its proper value. The spectra were dumped on magnetic tape at the end of each sequence and an asymmetry calculation was typed out. The asymmetry calculations and detector sums enabled the experimenter to spot any detector irregularities or target deterioration. The computer code continually monitored both the beam current and the solenoid current and stopped the data accumulation if anything went wrong.

B. Data Reduction

Preliminary asymmetry values and final values for data with well-separated neutron groups were calculated in the following manner. Let N(I) represent the number of counts in channel I. The indices U or D, and F or R denote the particular combination of up or down detectors and forward or reverse solenoid current which that particular spectrum represents.

The parameter a is then defined as

$$a = \left[\frac{\Sigma N_{UF}(I) \cdot \Sigma N_{UR}(I)}{\Sigma N_{DF}(I) \cdot \Sigma N_{UR}(I)}\right]^{1/2}$$

where the summation is over the channels of interest. The asymmetry is then given by

$$\epsilon = \frac{a - 1}{a + 1}$$

This particular method has the distinct advantage that the parameter α is independent of the detector efficiences as long as they are constant. (The detectors were shielded to prevent any dependence on the magnetic field.) The parameter α represents sort of a 'Left-Right' ratio in analogy with the traditional Left-Right asymmetry measurements. In fact, for the spectra which were fitted with Gaussian peaks, the spectra were first combined into a left spectrum and a right spectrum according to

$$N_{Left}(I) = 2\left[N_{UF}(I) \cdot N_{DR}(I)\right]^{1/2}$$

and

$$N_{Right}(I) = 2\left[N_{UR}(I) \cdot N_{DF}(I)\right]^{1/2} \quad .$$

Most of the asymmetry data were extracted by fitting the gated He-recoil spectra with calculated distributions composed of Gaussian peaks on a suitable background. Figure 3 shows a $^{9}Be(\alpha,n)$ summed spectrum from our earlier work.[6] The summed spectrum is formed by adding all the foreground spectra and subtracting the accidental background. This figure demonstrates how well a Gaussian line shape describes the data. The general procedure for extracting the asymmetries was to combine the eight original spectra into a "Left" spectrum and a "Right" spectrum as described above. These two spectra were then fitted independently (but with the same energies and resolution parameters). The asymmetries of the amplitudes of the Gaussian peaks are the values which are reported. The lower frame of Fig. 3 shows how well this procedure describes the measured channel by channel asymmetry, the solid curve representing a calculated fit.

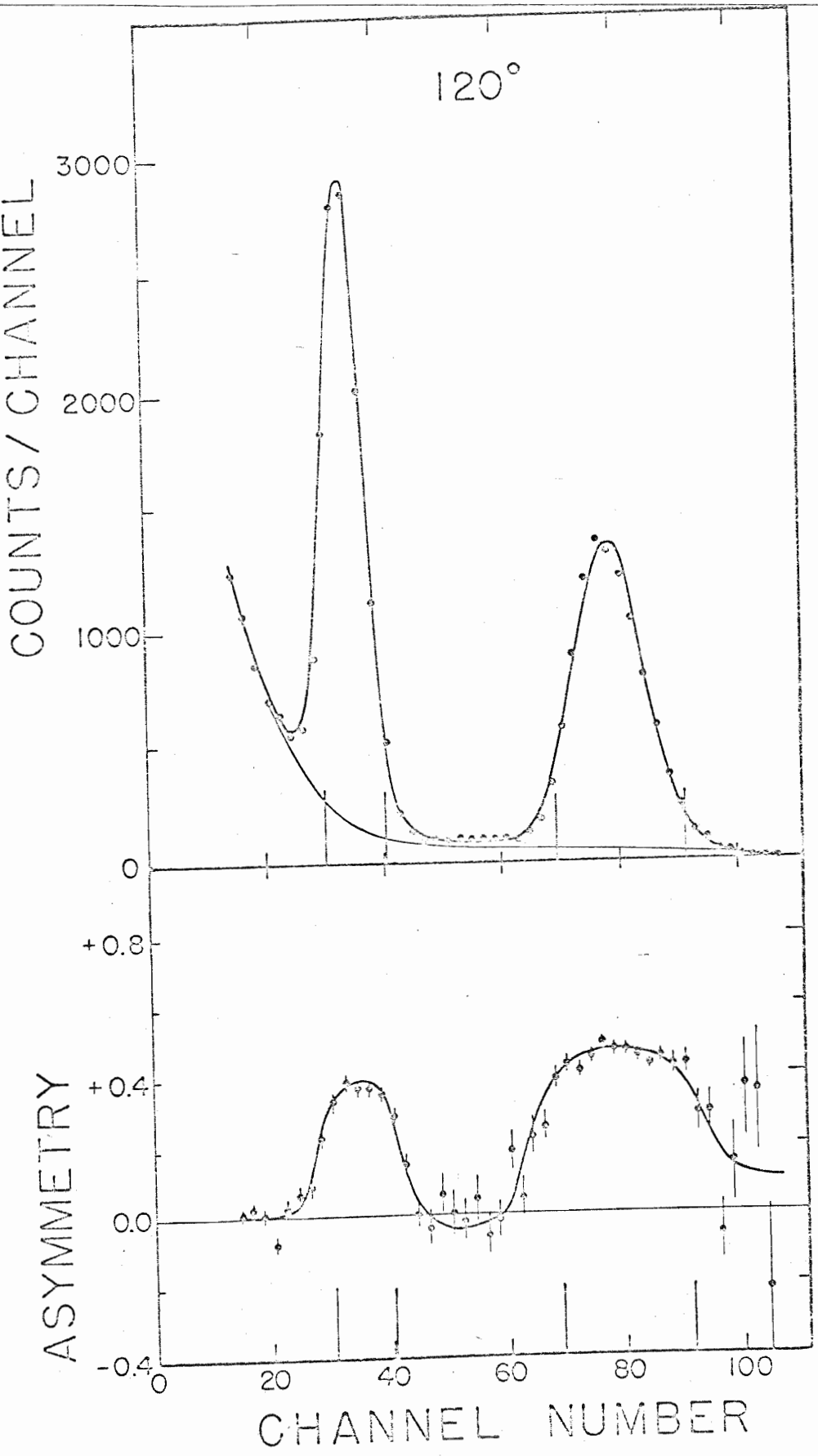

Figure 3. Typical Summed Spectrum and Channel by Channel Asymmetry with Fit for the ^{9}Be(α,n) Reaction at 2.55 MeV.

Two computer codes were used to fit the spectra. The first of these is the program PROMETHEUS,[4,7] which was written by R. S. Thomason and M. M. Meier. It operates on the IBM 360/75 computer and is the more powerful of the two programs. A second program (ASP) was written by the author to run on the DDP-224 computer at TUNL. ASP is an interactive program which runs in 8K words of core storage. Because of its small size more of the work must be done by the operator, and this is provided for with a display tube and appropriate input. Its main advantage is that the operator can analyze his data in a much shorter period of time. The main disadvantage is that it contains no automatic search routine for the energy scale and resolution parameters. These parameters are varied by operator controlled switches and the X^2 is displayed along with the data. Here X^2 is defined by

$$X^2 = \sum_I \frac{(F(I) - N(I))^2}{N(I)}$$

where N is the experimental spectrum and F is the calculated fit to the data. Because only the amplitudes are fitted by the program, the calculated distribution is expressed as a linear function of its variables, and the problem reduces to solving a set of linear equations. There is no need for an iterative search procedure, which would be disturbingly long on a small computer. The program can search on a quadratic background and places the Gaussian peaks according to the kinematics of the reaction. A more detailed description of the program will be presented in Appendix A.

The polarization was computed from the asymmetry by multiplying by the spin precession factor SPF and dividing by the average analyzing power $\overline{P_2}$. The spin precession factor is defined by

$$SPF = (\sin\phi)^{-1} \quad ,$$

where ϕ is the angle through which the neutron spins are precessed out of the reaction plane by the magnetic field of the solenoid. The average analyzing power $\overline{P_2}$ was calculated by averaging the n-He analyzing power over the experimental geometry using the Monte Carlo scattering program of Stammbach et al.[6] The analyzing power was calculated from the phase shifts of Satchler et al.[13] below 20 MeV and the phase shifts of Hoop and Barschall[14] at higher energies.

Chapter III

THE $^{11}B(d,n)^{12}C$ REACTIONS

A. Introduction

The $^{11}B(d,n)$ reactions leading to the two lowest levels of ^{12}C are of particular interest in one-particle stripping because they are expected to demonstrate the j-dependence in stripping to the 1p shell. The $^{11}B(d,n_0)$ reaction proceeds through a $p_{3/2}$ transfer while the $^{11}(d,n_1)$ reaction may proceed through either a $p_{1/2}$ or a $p_{3/2}$ transfer. The shell model calculations of Cohen and Kurath[8] predict that it will be predominately $p_{1/2}$. A measurement of these two reactions should show the differences in stripping with angular momentum transfers of $j = \ell + s$ and $j = \ell - s$.

These reactions have been investigated between 3 and 4 MeV by Meier.[7] Meier et al.[9] have compared several reactions on 1p shell nuclei and have found that the $^{11}B(d,n_1)$ reaction does not conform to trends of $p_{1/2}$ stripping in neighboring nuclei at similar energies. In particular, $^{12}C(d,n)$, $^{12}C(d,p)$, $^{14}N(d,n)$, and $^{15}N(d,n)$ all show large negative polarizations near the main stripping peak (about 20° (c.m.)). The $^{11}B(d,n_1)$

polarization is fairly stable from 3 to 4 MeV and its sign is positive. The data of Meier[7] at 4 MeV are shown in the top frame of Fig. 4. The data show a strong j-dependence, but the empirical rule of Reber and Saladin,[10] and Meier et al.[9] that the $p_{1/2}$ transfers show considerably more negative polarizations than do $p_{3/2}$ transfers near the main stripping peak is not supported. Meier et al.[11] have suggested that this discrepancy might be caused by the high Q-values (13.7 and 9.3 MeV) of the two reactions. The high Q-values can produce a mismatch of the incoming and outgoing neutron momenta. A measure of the mismatch is the quantity

$$\vec{q} = \hbar\vec{k}_n - 1/2\,(\hbar\vec{k}_d)\,,$$

where $\hbar\vec{k}_n$ is the outgoing neutron momentum and $\hbar\vec{k}_d$ is the deuteron momentum. If q is large then the outgoing neutron must receive most of its momentum from the internal energy, or loosely speaking, from the internal deuteron wave function. Semiclassically at least, this requirement means that the neutron must be close to the proton at the time the stripping takes place. As is pointed out by D. H. Wilkinson,[12] this condition can cause two things to happen. Compound nucleus formation is enhanced because both the neutron and the proton are near the nucleus. Secondly, the nucleus may be distorted by the presence of the extra nucleon and the simple stripping theory may not be applicable. The momentum mismatch q varies from about 100 to 300 MeV/c for the $^{11}B(d,n_1)$ reaction and is even worse for the n_0 group. With the high momenta involved it may not be too surprising that the polarization distributions observed by Meier[7] are unusual.

Figure 4. The $^{11}B(d,n_0)$ and $^{11}B(d,n_1)$ Polarization Distributions.

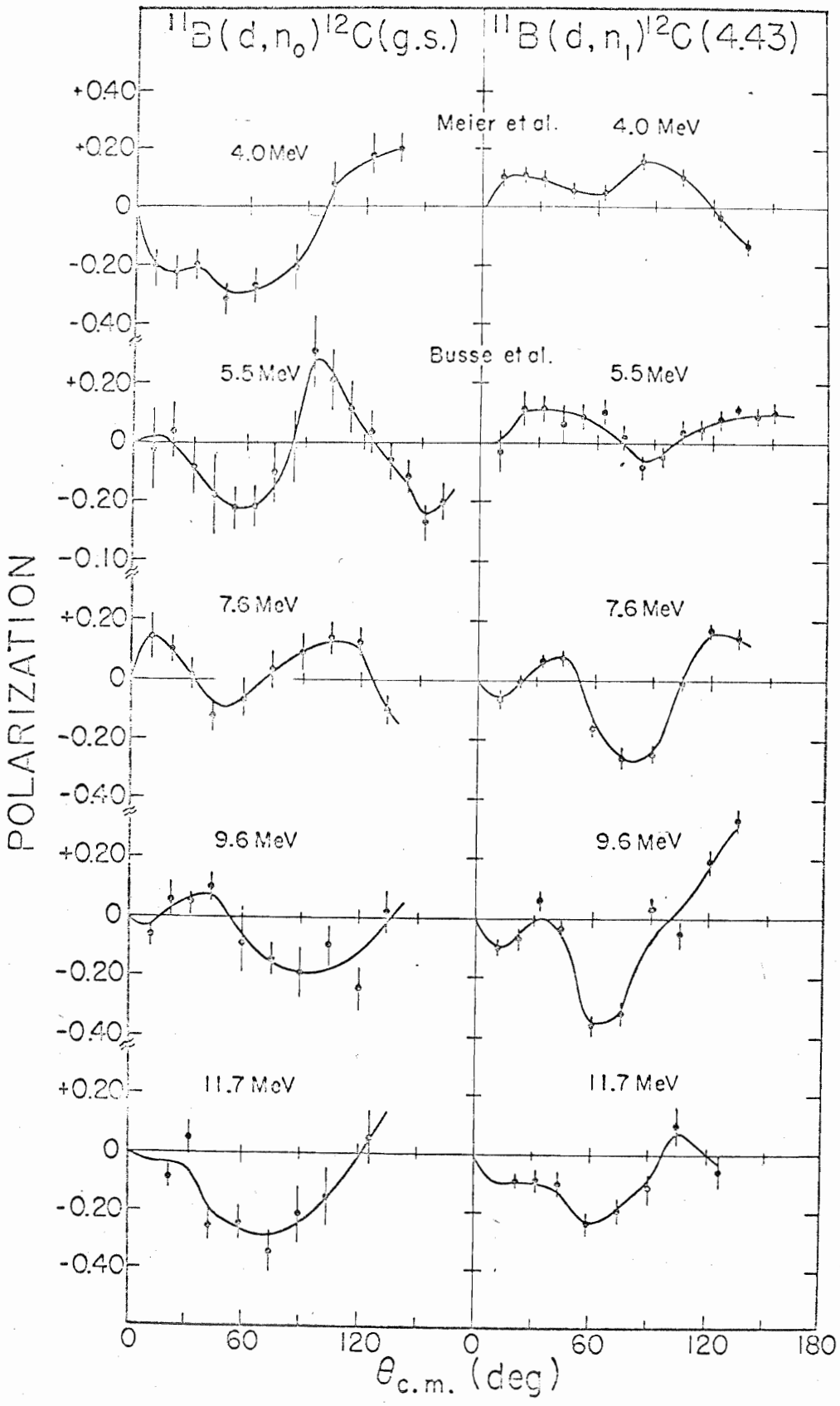
$^{11}B(d,n_0)^{12}C(g.s.)$
$^{11}B(d,n_1)^{12}C(4.43)$
Meier et al.
Busse et al.
4.0 MeV
5.5 MeV
7.6 MeV
9.6 MeV
11.7 MeV
POLARIZATION
$\theta_{c.m.}$ (deg)
+0.40
+0.20
0
-0.20
-0.40
-0.10
60
120
180

In the present measurements the neutron polarization angular distributions were obtained at 7.6, 9.6, and 11.7 MeV in order to investigate their behavior at higher energies. Differential cross section distributions were measured at three energies in order to facilitate the stripping analysis.

B. Experimental Details

Targets for the polarization measurements were made by depositing a slurry of natural amorphous boron and distilled water onto tantalum endcaps. The mixture was allowed to dry slowly and was weighed after heating the target for several minutes. The targets presented energy losses of from 600 to 800 keV to the incident deuteron beam. They were surprisingly durable and suffered little deterioration when exposed to the beam for long periods. There were no contaminant problems as the Q-values for the first two neutron groups (13.7 and 9.3 MeV) were higher than the Q-values of any of the possible contaminants.

The polarimeter was essentially that described in chapter II, except no solenoid was used for spin precession because of a delay in setting it up in the tandem laboratory. The side detectors were therefore mounted in the horizontal plane, and instead of reversing the magnetic field, the reaction angle was changed from $+\theta_1$ to $-\theta_1$. This essentially reversed the roles of the two side detectors, but more care had to be taken to shield the side detectors from the direct neutron flux. A gain shift can occur with

drastic counting rate changes, and this can lead to false asymmetries if steps are not taken to prevent this. The side detectors were plastic scintillators (5.1 X 7.6 X 15.3 cm^3) and were mounted 19 cm (center-to-center) from the helium cell.

The asymmetry data were extracted by fitting the spectra with Gaussian line shapes as described in chapter II. Figure 5 shows an example of one of the fits to the summed spectrum. The asymmetry data were divided by the analyzing power of the polarimeter as calculated using the phase shifts of Satchler et al.[13] below 20 MeV and those of Hoop and Barschall[14] above 20 MeV to yield the polarizations. Two of the (d,n_0) data points were close to the ^4He+n resonance at 22.15 MeV. These points were 85° (lab) at 11.7 MeV and 55° (lab) at 9.6 MeV. For these points the average analyzing power is uncertain and the error bars have been increased to compensate for this. A tabulation of the polarization data is presented in table 1.

A comparison of the present data with the data of Meier[7] at 4 MeV and Busse et al.[15] at 5.5 MeV is presented in Figure 4. The sign of the polarization here as in the rest of this dissertation is consistent with the Basel convention. The solid lines serve as a guide to the eye and have no other significance except at 4 MeV where they represent an average of the data from 3 to 4 MeV. Both groups show a slow change with energy over the region, but the n_1 group changes in a more regular fashion. The dip around 60° (c.m.) simply deepens until at the higher energies the distribution assumes a shape similar to the $p_{1/2}$ transfers of neighboring nuclei seen by Meier[7] at lower energies. The higher energy distributions show

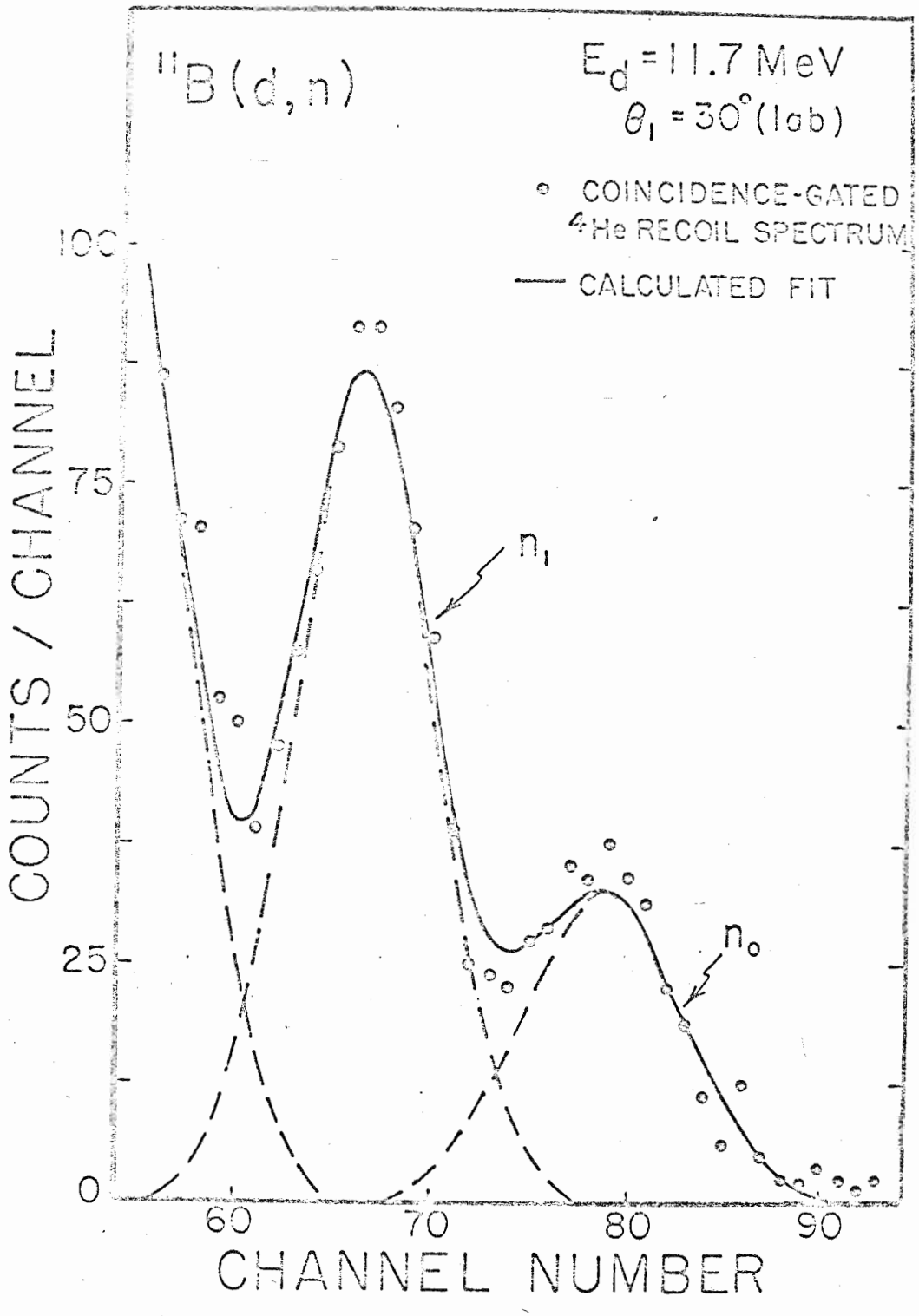

Figure 5. Typical Summed Spectrum and Fit for the $^{11}B(d,n)$ Reaction.

Table 1. The $^{11}B(d,n_0)$ and $^{11}B(d,n_1)$ Polarizations.

			$^{11}B(d,n_0)$				$^{11}B(d,n_1)$		
E_d	$\theta_{lab}^{(deg)}$	$\theta_{C.M}^{(deg)}$	Asymmetry	$\overline{P_2}$	Polarization	$\theta_{C.M.}^{(deg)}$	Asymmetry	$\overline{P_2}$	Polarization
7.6	10	10.7	0.125 ± 0.065	0.86	0.145 ± 0.076	10.8	-0.058 ± 0.027	0.86	-0.067 ± 0.031
7.6	20	21.4	0.091 ± 0.036	0.86	0.105 ± 0.042	21.6	-0.002 ± 0.019	0.86	-0.002 ± 0.022
7.6	30	32.0	0.015 ± 0.044	0.86	0.017 ± 0.052	32.3	0.052 ± 0.018	0.86	0.061 ± 0.021
7.6	40	42.6	-0.107 ± 0.047	0.86	-0.124 ± 0.055	43.0	0.064 ± 0.025	0.86	0.075 ± 0.029
7.6	55	58.3	-0.059 ± 0.046	0.86	-0.069 ± 0.054	58.8	-0.137 ± 0.027	0.86	-0.160 ± 0.031
7.6	70	73.8	0.028 ± 0.056	0.86	0.032 ± 0.066	74.3	-0.224 ± 0.031	0.86	-0.262 ± 0.036
7.6	85	89.1	0.077 ± 0.054	0.86	0.090 ± 0.063	89.6	-0.213 ± 0.025	0.86	-0.248 ± 0.029
7.6	100	104.0	0.118 ± 0.045	0.86	0.138 ± 0.052	104.5	-0.009 ± 0.024	0.86	-0.011 ± 0.028
7.6	115	118.7	0.107 ± 0.048	0.86	0.125 ± 0.047	119.2	0.142 ± 0.023	0.86	0.166 ± 0.027
7.6	130	133.1	-0.087 ± 0.040	0.86	-0.102 ± 0.046	133.5	0.123 ± 0.027	0.86	0.143 ± 0.032
9.6	10	10.8	-0.052 ± 0.034	0.82	-0.063 ± 0.042	10.8	-0.086 ± 0.024	0.88	-0.098 ± 0.027
9.6	20	21.5	0.048 ± 0.050	0.82	0.059 ± 0.061	21.7	-0.064 ± 0.021	0.88	-0.073 ± 0.037
9.6	30	32.2	0.040 ± 0.027	0.82	0.049 ± 0.033	32.5	0.054 ± 0.025	0.88	0.061 ± 0.028
9.6	40	42.8	0.079 ± 0.039	0.81	0.098 ± 0.048	43.2	-0.032 ± 0.021	0.88	-0.036 ± 0.024
9.6	55	58.6	-0.062 ± 0.044	0.70	-0.088 ± 0.10	59.0	-0.315 ± 0.033	0.87	-0.360 ± 0.037
9.6	70	74.1	-0.126 ± 0.048	0.88	-0.142 ± 0.054	74.6	-0.279 ± 0.035	0.87	-0.320 ± 0.040
9.6	85	89.4	-0.165 ± 0.074	0.88	-0.187 ± 0.085	89.9	0.032 ± 0.056	0.87	0.037 ± 0.065
9.6	100	104.3	-0.087 ± 0.062	0.88	-0.098 ± 0.070	104.8	-0.046 ± 0.035	0.87	-0.053 ± 0.040
9.6	115	119.0	-0.212 ± 0.068	0.88	-0.241 ± 0.078	119.5	0.167 ± 0.037	0.87	0.191 ± 0.043
9.6	130	133.4	0.018 ± 0.059	0.88	0.020 ± 0.068	133.8	0.288 ± 0.035	0.87	0.330 ± 0.040

Table 1 (continued)

			$^{11}B(d,n_0)$				$^{11}B(d,n_1)$		
E_d	$\theta_{lab}^{(deg)}$	$\theta_{C.M.}^{(deg)}$	Asymmetry	P_2	Polarization	$\theta_{C.M.}^{(deg)}$	Asymmetry	P_2	Polarization
11.7	20	21.6	-0.071 ± 0.034	0.84	-0.085 ± 0.041	21.8	-0.076 ± 0.018	0.88	-0.087 ± 0.020
11.7	30	32.3	0.040 ± 0.048	0.84	0.048 ± 0.057	32.6	-0.074 ± 0.035	0.88	-0.084 ± 0.040
11.7	40	43.0	-0.210 ± 0.046	0.84	-0.250 ± 0.055	43.3	-0.083 ± 0.038	0.88	-0.094 ± 0.043
11.7	55	58.8	-0.205 ± 0.051	0.83	-0.240 ± 0.062	59.2	-0.206 ± 0.035	0.88	-0.234 ± 0.040
11.7	70	74.4	-0.279 ± 0.062	0.82	-0.340 ± 0.075	74.9	-0.165 ± 0.039	0.88	-0.188 ± 0.045
11.7	85	89.7	-0.126 ± 0.060	0.60	-0.210 ± 0.100	90.2	-0.099 ± 0.045	0.88	-0.114 ± 0.051
11.7	100	104.6	-0.132 ± 0.089	0.89	-0.150 ± 0.100	105.1	0.092 ± 0.054	0.87	0.105 ± 0.062
11.7	120	124.0	0.051 ± 0.082	0.88	0.058 ± 0.092	124.5	-0.049 ± 0.047	0.87	-0.056 ± 0.054

little j-dependence, and the experimental observation that $p_{1/2}$ transfers are much more negative near the main stripping peak is still unsupported in this reaction. Of course, it is somewhat uncertain just how small the $p_{3/2}$ contribution to the n_1 reaction really is.

The present data at 9.6 MeV are in fair agreement with the data of Smotryaev and Trostin[16] at 9.3 MeV. The data are hard to compare exactly as the Russian data had a deuteron energy spread of 2.4 MeV, and as is seen in the present results, this range is enough to average over significant changes. It should be remarked also that all of their $^{11}B(d,n_0)$ data were kinematically within range of the ^4He+n resonance at 22.15 MeV.

Differential cross section measurements were obtained for two reasons. First, a knowledge of the angular distributions is necessary for the stripping analysis. Secondly, an early 0° excitation function of Almond and Risser[17] showed resonances in this energy region. In particular, their results indicated a possible resonance at 9.6 MeV. It was important to know if any appreciable structure would show up which might affect the data of the present polarization measurements which employed thick targets. The present cross section data were taken with a natural boron target with a thickness corresponding to a 200 keV energy loss at about 9 MeV. Recoil spectra were recorded with the helium scintillator in short runs of about 5 minutes duration. The cross section information was extracted by fitting the high energy part of the spectrum with a recoil energy distribution calculated from the n-α phase shifts of Stammbach.[8] The calculated distribution

was smeared with the intrinsic resolution of the helium cell and fit to that part of the n_0 recoil spectrum which extended beyond the n_1 group. The normalization factor is proportional to the cross section. The calculated n_0 spectrum was then subtracted from the data and the process was repeated for the n_1 group. The two groups were not fit simultaneously because of space limitations in the computer. This method works quite well for two well-separated groups, but it should probably not be used for any more than two groups without fitting them simultaneously. Figure 6 shows a typical recoil spectrum with its fitted distribution. The deviation below channel 70 is associated with lower energy neutron groups which were not included.

Results of the angular distribution measurements are shown in Fig. 7 for 6.9, 9.6, and 11.7 MeV and are tabulated in Table 2. All of the cross section data are expressed in the center of mass system and are normalized to the data of Almond and Risser[17] using their data point at 9 MeV, 20° (lab). The value of this point was taken to be 1.0 mb/sr. The present data therefore correspond to mb/sr if one accepts this normalization.

Strong stripping patterns for both neutron groups are quite evident The n_0 distribution at the lowest energy exhibits a strong back angle cross section which is characteristic of this reaction at low energies.[15,17] There are two uncertain points for the n_0 group because of the $^4He + n$ resonance at 22.15 MeV. They are 85° (lab) at 11.7 MeV and 50° (lab) at 9.6 MeV.

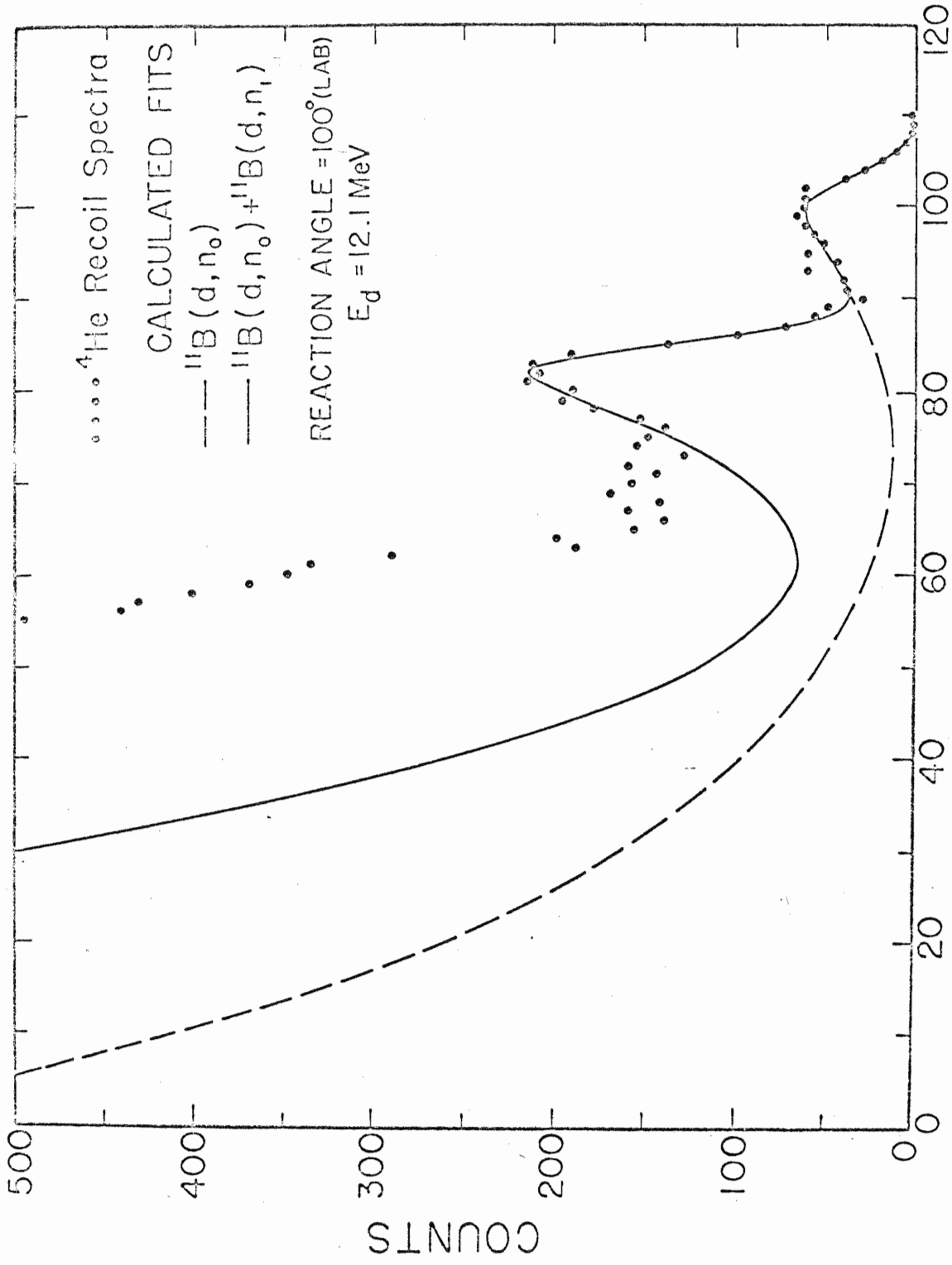

Figure 6. Typical He-recoil Spectrum and Fit for ^{11}B(d,n).

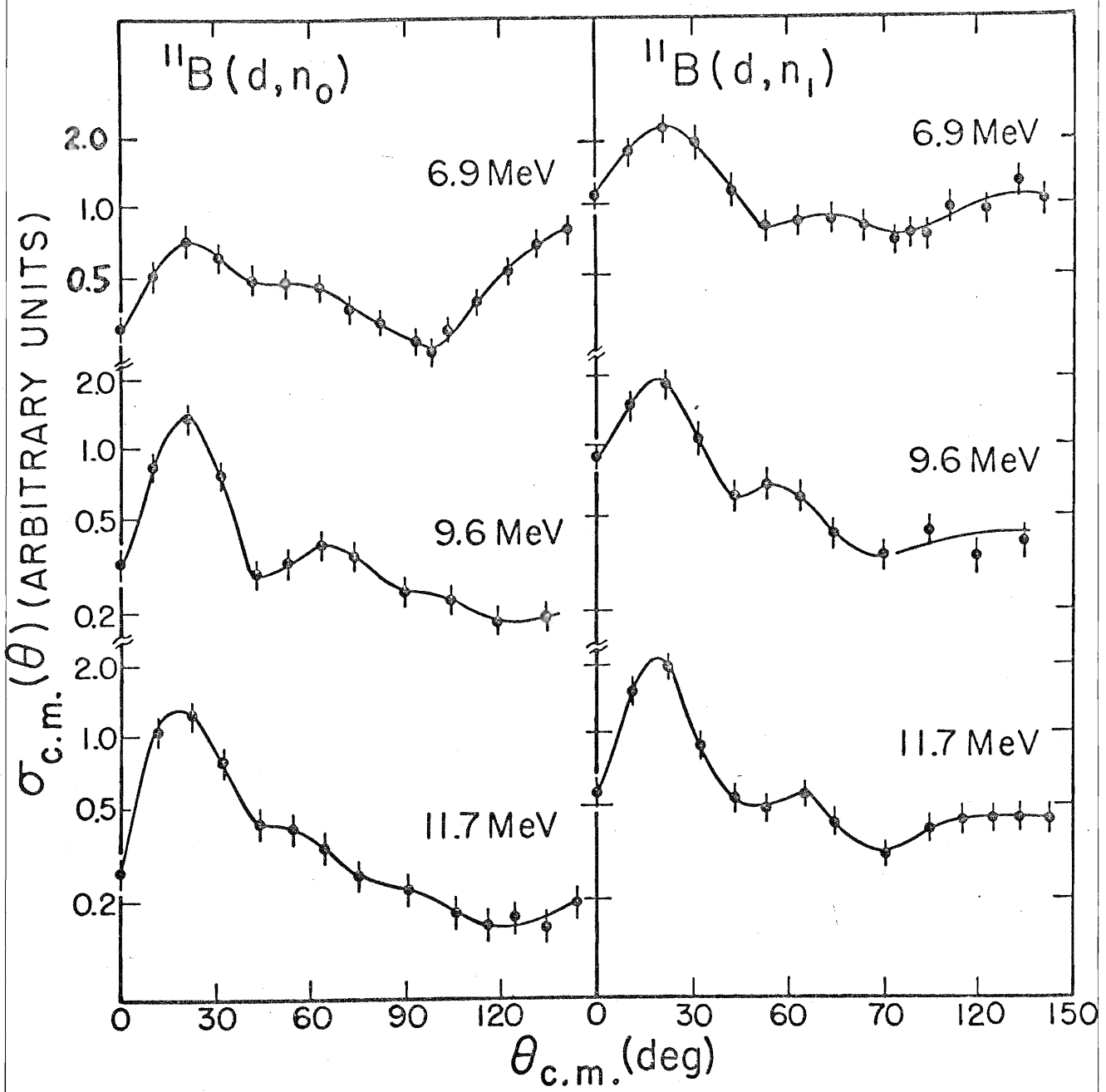

Figure 7. The $^{11}B(d,n_0)$ and $^{11}B(d,n_1)$ Angular Distributions.

Table 2. $^{11}B(d,n_0)$ and $^{11}B(d,n_1)$ Relative Cross Section Angular Distributions.

	E_d = 6.9 MeV				E_d = 9.6 MeV				E_d = 11.7 MeV			
	n_0		n_1		n_0		n_1		n_0		n_1	
θ_{lab} (deg)	$\theta_{C.M.}$	σ	$\theta_{C.M.}$ (deg)	σ	$\theta_{C.M.}$ (deg)	σ	$\theta_{C.M.}$ (deg)	σ	$\theta_{C.M.}$ (deg)	σ	$\theta_{C.M.}$ (deg)	σ
0	0.0	0.30	0.0	1.05	0.0	0.33	0.0	0.90	0.0	0.49	0.0	0.90
10	10.7	0.51	10.8	1.63	10.8	0.84	10.8	1.45	10.8	1.06	10.9	1.49
20	21.4	0.72	21.5	2.07	21.5	1.34	21.7	1.80	21.6	1.27	21.8	1.92
30	32.0	0.62	32.2	1.79	32.2	0.78	32.5	1.07	32.3	0.79	32.6	0.88
40	42.6	0.51	42.9	1.11	42.8	0.29	43.2	0.59	43.0	0.42	43.3	0.53
50	53.0	0.49	53.4	0.78	53.4	0.32	53.8	0.68	53.6	0.41	54.0	0.47
60	63.4	0.45	63.9	0.81	63.8	0.39	64.3	0.61	64.0	0.34	64.5	0.55
70	73.7	0.36	74.2	0.83	74.1	0.35	74.6	0.43	74.4	0.25	74.9	0.42
80	83.9	0.32	84.4	0.78								
85					89.4	0.24	89.9	0.34	89.7	0.23	90.2	0.30
90	94.0	0.27	94.5	0.68								
95	98.9	0.28	99.5	0.72								
100	103.9	0.30	104.4	0.71	104.3	0.22	104.8	0.42	104.6	0.18	105.1	0.39
110	113.7	0.38	114.2	0.92					114.4	0.16	114.9	0.43
115					119.0	0.18	119.5	0.34				
120	123.4	0.51	123.9	0.93					124.0	0.17	124.5	0.42
130	133.0	0.68	133.4	1.19	133.4	0.19	133.8	0.38	133.6	0.16	134.0	0.44
140	142.5	0.78	142.9	0.97					143.0	0.20	143.3	0.43

They are 85° (lab) at 11.7 MeV and 50° (lab) at 9.6 MeV. The differential cross section excitation functions which were obtained at 0°, 20°, and 100° (lab) are tabulated in Table 3 and plotted in Fig. 8. Three data points for the 20° excitation function are omitted because of the ^{4}He + n resonance. Considering the overall accuracy of these measurements (about 15%), no structure is evident from these excitation functions. In particular, the "one-point resonance" seen by Almond and Risser[17] at 9.6 MeV is not seen with the 200 keV target.

C. Analysis

It was hoped early in the analysis that the DWBA calculations could be made entirely with published optical model (OM) potentials for both the entrance and exit channels. The calculations turned out to be relatively insensitive to the details of the neutron potential, so this channel presented much less of a problem than the entrance channel. The published deuteron sets failed to describe the reaction data completely and were abandoned. It was decided to generate OM deuteron sets from the elastic data and to try these sets on the (d,n) data. There is, of course, no guarantee that the wave functions in the nuclear interior are adequately described in this manner. A search on both the elastic and reaction data was not attempted because the DWBA calculations are appreciably longer than the elastic calculations alone and the procedure would have been prohibitively

Table 3. $^{11}B(d,n_0)$ and $^{11}B(d,n_1)$ Relative Cross Section Excitation Functions.

E_d (MeV)	$\theta_{lab} = 0^\circ$		$\theta_{lab} = 20^\circ$		$\theta_{lab} = 100^\circ$	
	σ_{n_0}	σ_{n_1}	σ_{n_0}	σ_{n_1}	σ_{n_0}	σ_{n_1}
6.9	0.34	1.17	0.80	2.48	0.28	0.69
7.1			0.81	2.54	0.28	0.68
7.3			0.80	2.41	0.26	0.64
7.5			0.90	2.26	0.25	0.67
7.7			0.89	2.30	0.26	0.59
7.9			1.00	2.20	0.26	0.55
8.1			1.06	2.14	0.26	0.51
8.3			1.16	2.22	0.30	0.48
8.5			1.23	2.17	0.25	0.49
8.7	0.56	0.95	1.09	2.34	0.26	0.47
8.9	0.48	0.96	1.01	2.18	0.25	0.50
9.1	0.51	1.09	1.00	2.03	0.24	0.48
9.3	0.42	1.08	1.33	1.99	0.23	0.48
9.5	0.38	1.01	1.33	2.02	0.23	0.48
9.7	0.33	0.90	1.36	2.07	0.21	0.46
9.9	0.34	0.78	1.43	2.06	0.22	0.42
10.1	0.32	0.75	1.28	2.22	0.20	0.41
10.3	0.29	0.81	2.09	2.33	0.19	0.40
10.5	0.22	0.73	1.30	2.11	0.19	0.42
10.7	0.37	0.70	1.25	2.20	0.18	0.41
10.9	0.30	0.66	1.39	2.12	0.19	0.42
11.1	0.25	0.59	1.18	2.18	0.20	0.42
11.3	0.24	0.74	1.55	2.15	0.19	0.40
11.5	0.24	0.81	1.47	2.18	0.21	0.38
11.7	0.31	0.71	1.50	2.17	0.18	0.39
11.9	0.31	0.74	1.50	2.08	0.20	0.37
12.1					0.20	0.36

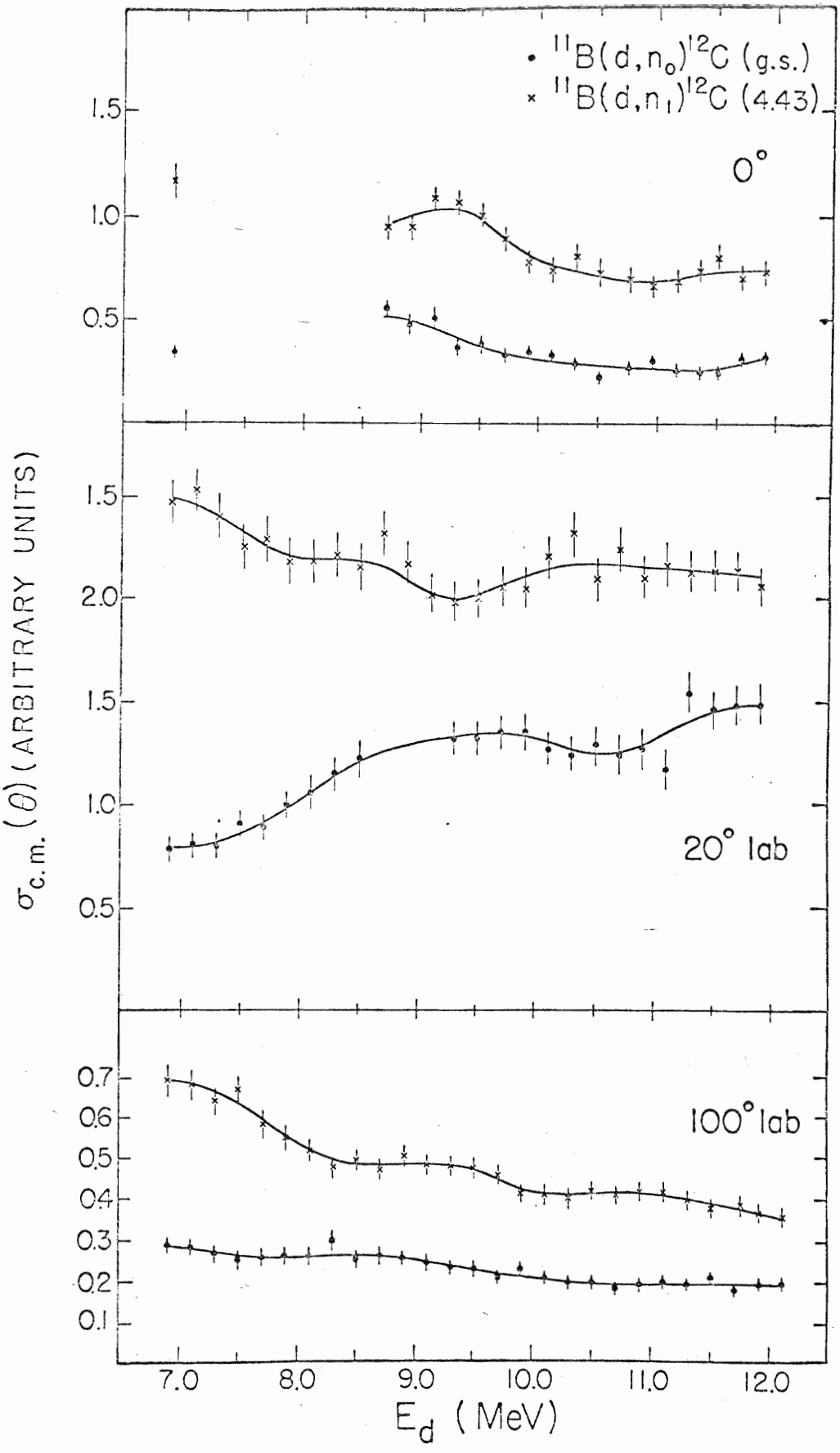

Figure 8. The $^{11}B(d,n_0)$ and $^{11}B(d,n_1)$ Relative Cross Section Excitation Functions.

expensive. At the time the analysis was started the only elastic data available was that of Fitz et al.[19] at 11.8 MeV. It was decided that more elastic scattering data were needed, so angular distributions at 7.5 and 9.5 MeV were measured at our laboratory by R. A. Hardekopf et al.[20] The data are tabulated in Appendix B, and are plotted in Fig. 9.

The three elastic scattering distributions were analyzed using the on-line computer code OPTICS of R. A. Hardekopf.[20] The form of the OM potentials used in this analysis is given by

$$V(r) = V_{coul}(r) - V\, f(r, r_o, a_o) + 4\, i\, a_i\, W \frac{d}{dr}\left(f(r, r_i, a_i)\right)$$

$$+ \left(\frac{\hbar}{M_\pi c}\right)^2 V_{so}\, 2\,(\ell \cdot S)\, \frac{1}{r} \frac{d}{dr}\left(f(r, r_{so}, a_{so})\right)$$

where

$$f(r, r', a') = \left[1 + \exp\left(\frac{(r-r')}{a'} A^{1/3}\right)\right]^{-1} .$$

The forward angle data were weighted more heavily in the analysis because of uncertainties associated with compound nucleus contributions where the absolute cross section is low. The effect of the compound nucleus was approximated in the program by a Hauser-Feshbach contribution calculated in a manner suggested by Thompson[21] with a spin cutoff factor of $\sigma^2 = 9$ and a normalization $D_o/\Gamma_o = 0.4$. No attempt was made to optimize these parameters. Because the data were available at only three energies, no attempt was made to force a smooth energy variation of the OM parameters. The spin-orbit term made little difference in the calculations and so was not searched on. It was set at 9 MeV, a value obtained from the work of Schwandt and Haeberli[22] on ^{40}Ca(d,d). The parameter r_{so} was generally

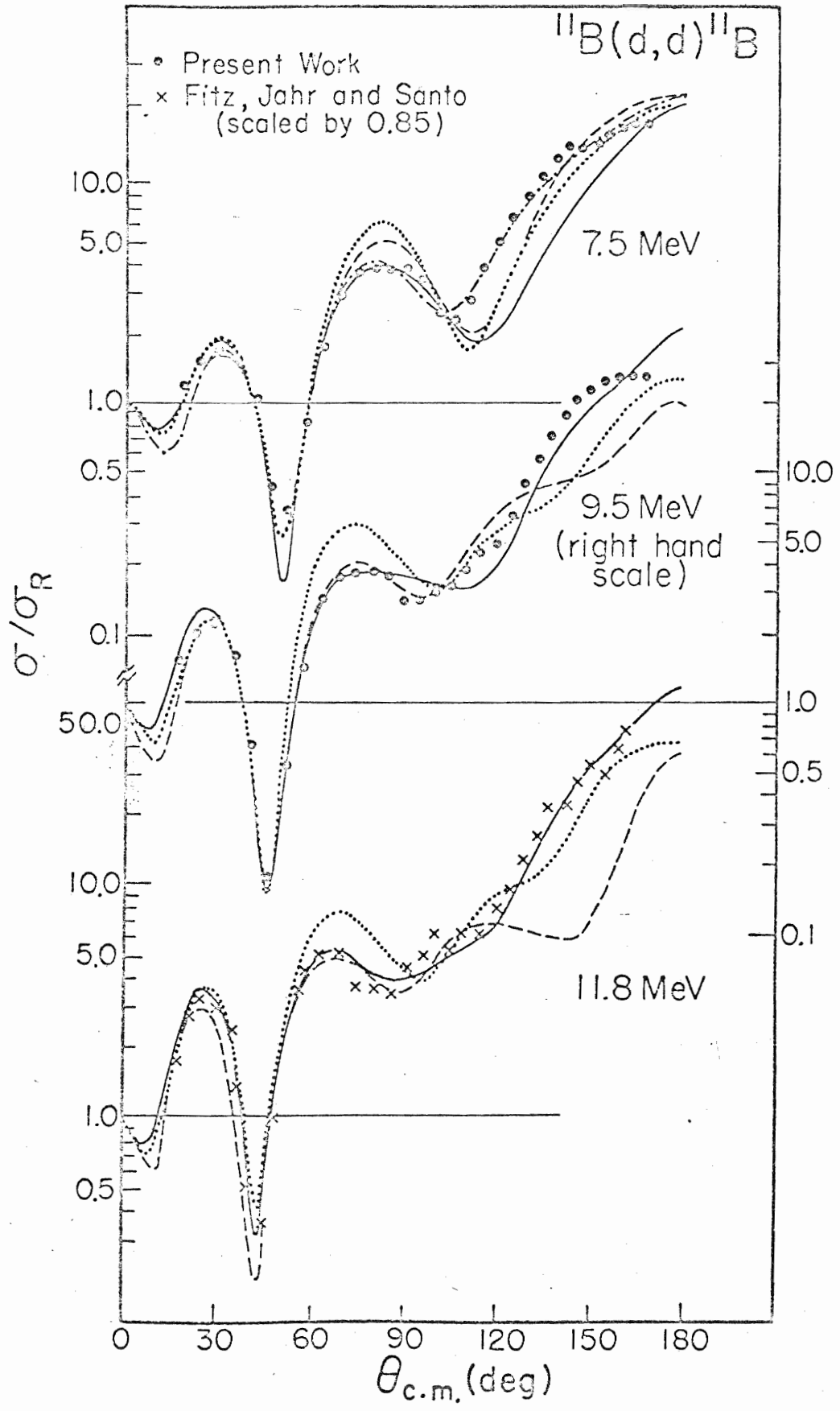

Figure 9. The $^{11}B(d,d)$ Elastic Scattering Cross Sections and Optical Model Fits.

kept at a value near the corresponding radius parameter of the real well.

The potentials were characterized for tabulating purposes by their values of V and r_0. Corresponding to the well known Vr_0^n ambiguity, sets with about the same product $Vr_0^{1.4}$ were considered to be of the same type. In general, three types of potentials were found that adequately described the elastic scattering data. Potentials of type I (represented by the solid lines in Fig. 9) were characterized by a well depth V of about 105 MeV and a radius r_0 around 1.05 fm. Type II potentials (dashed and dot-dashed curves) had a depth V of about 105 MeV and an r_0 of approximately 1.2 fm. Both of these types required that the 11.8 MeV distribution of Fitz et al.[19] be normalized to about 0.85 times its reported value. They both described the data far better than those of type III (dotted curves), which had a V of about 110 MeV and an r_0 near 1.65 fm. The type III potentials generally gave inferior fits, and the cross section was consistently overestimated, especially in the region around 60° (c.m.). The overall normalization had to be forced down by using a very small diffuseness for the imaginary well. The OM potentials listed in Table 4 represent the best fits to the elastic data for each type of potential. Potential 7.5b is somewhat anomalous since no corresponding potentials were found at the higher energies.

The DWBA calculations were made using the code DWUCK of P. D. Kunz.[23] The neutron potential was taken from the work of Watson et al.[24] and is included in Table 4. The calculations were relatively in-

Table 4. OM Parameter Sets for $^{11}B + d$ and $^{12}C + r$.

No.	Particle	Type	V	r_0	a_0	W_d	r_i	a_i	V_{so}	r_{so}	a_{so}
7.5a	d	I	106	1.05	0.70	4.0	1.35	1.20	9.0	0.90	0.80
7.5b	d	II'	111	1.11	0.81	8.7	1.05	0.81	9.0	1.10	0.80
7.5c	d	II	95	1.20	0.88	15.0	1.85	0.35	9.0	1.20	1.00
7.5d	d	III	110	1.65	0.65	30.0	2.00	0.25	9.0	1.30	0.60
9.5a	d	I	105	1.00	0.75	3.2	1.50	1.30	9.0	1.00	0.80
9.5b	d	II	105	1.20	0.88	20.0	1.70	0.38	9.0	1.20	1.00
9.5c	d	III	115	1.65	0.60	35.0	1.80	0.25	9.0	1.30	0.60
11.8a	d	I	103	1.05	0.77	4.0	1.4	1.10	9.0	1.10	0.80
11.8b	d	II	110	1.20	0.88	24.0	1.60	0.41	9.0	1.20	1.00
11.8c	d	III	110	1.70	0.55	35.0	1.80	0.22	9.0	1.30	0.60
N-1	n		54	1.13	0.57	8.4	1.13	0.50	5.5	1.13	0.57

sensitive to the details of the neutron well. The results of the DWBA calculations were in general discouraging. Agreement with the experimental data was minimal for all three types of deuteron potentials. The results for deuteron potentials of type I (solid lines) and type II (dashed lines) are shown in Fig. 10. The calculated cross sections are adjusted in the figure so that the peaks of the type I calculations are at the same level as the experimental data. Again, the scales on the left corresponds to mb/sr if the calibration of Almond and Risser[17] is used. The scales for the calculated cross sections are on the right. (These scales do not include the spin factors. These are introduced later in the discussion on spectroscopic factors.) The curves for the type II calculations at the lowest energy are with the anomalous set 7.5b, as the regular type II potential gave inferior results. Calculations for the type III deuteron potentials gave poor descriptions of the data and are not displayed as the quality of the fits to the elastic data suggest that this is probably not a reasonable type of potential. Except as noted otherwise, the calculations were done using the finite-range and non-local potential approximations incorporated in the code DWUCK. The program approximates the effect of the finite range of the n-p interaction by including a factor

$$W(r) = \left[1 + \frac{2}{\hbar^2} \frac{m_n m_p}{m^d} R^2 \quad V_d(r) - V_p(r) - V_n(r) - S.E._{np}\right]^{-1}$$

in the radial integrals. Here m_n, m_p, and m_d are the masses of the neutron, proton, and deuteron, respectively. The V_n, V_p, and V_d are their

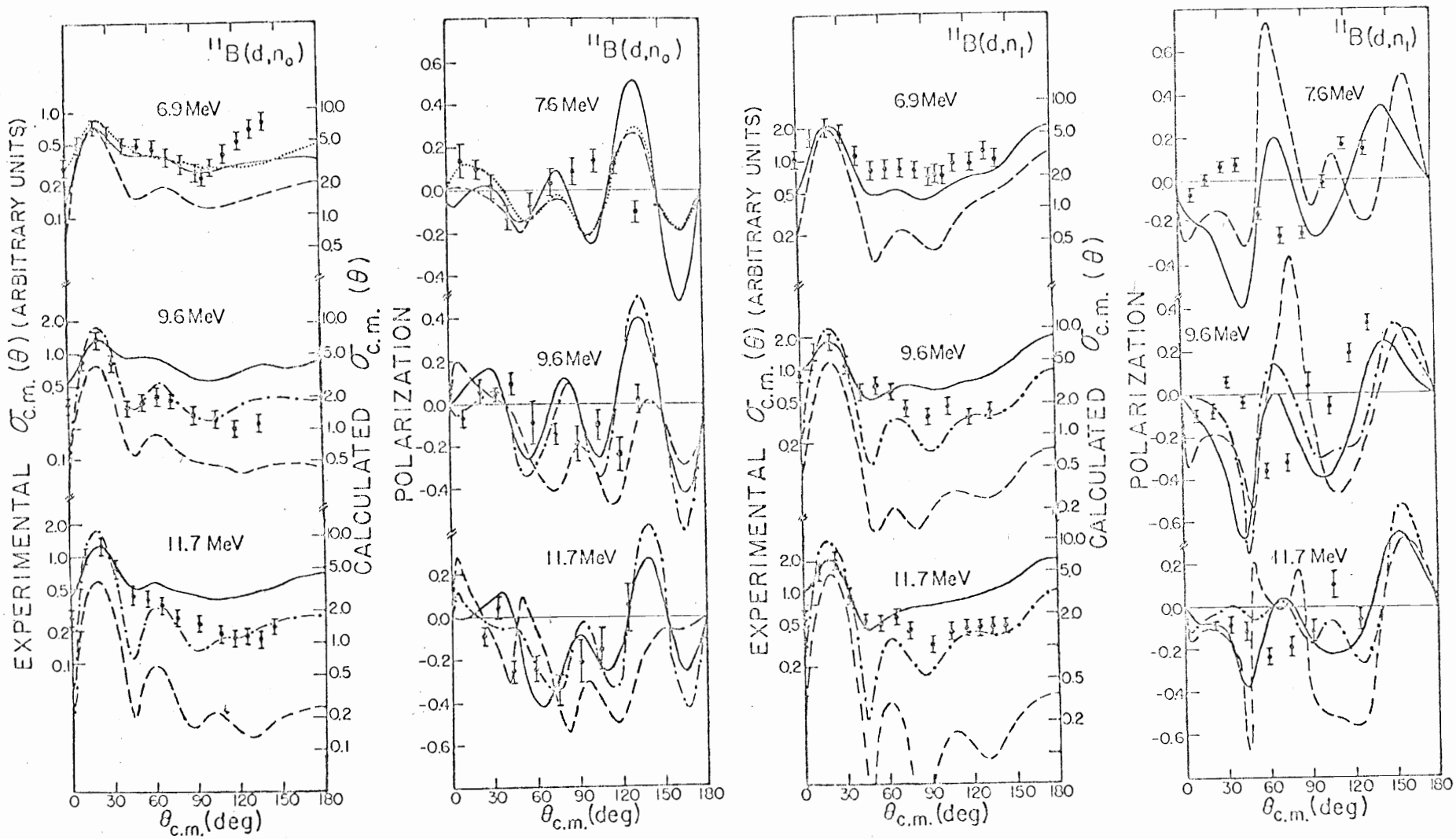

Figure 10. Results of the DWBA Calculations for $^{11}B(d,n_0)$ and $^{11}B(d,n_1)$.

respective potentials, and S. E.$_{np}$ is the separation energy of the neutron from the proton. The parameter R is the finite-range parameter and was taken to be 0.621 fm. In a similar manner correction was made for non-local effects by including in the radial integrals a factor for each potential (including the bound state) of the form

$$W(r) = \left[1 - \frac{\beta^2}{4} \frac{2m}{\hbar^2} V(r)\right]^{-1/2}$$

The non-local parameter β was taken to be 0.54 for the deuteron and 0.85 for the nucleon. The results were insensitive to changes in the bound state well, which had an r_0 of 1.15 fm and an a_0 of 0.57 fm.

Of the finite range, non-local calculations for types I and II several things are evident. The polarization for the n_0 group is much better described than that for the n_1 group. (Calculations with a $p_{3/2}$ transfer were also tried for the n_1 group, but agreement was still poor.) The type I cross sections (solid curves) are larger than those of type II (dashed curves), and the type II cross sections show a much stronger angular dependence. The type II polarizations are generally wild when the cross section is low. The type I deuteron potentials seem more consistent with the n_0 polarizations, but agreement is still far from satisfactory, especially at the middle energy. Variations on the deuteron spin-orbit potential were tried but did not seem to help appreciably. The effect of doing the calculations in zero range, local approximations is demonstrated by the dotted curve for the lowest energy distribution using the anomalous set 7.5b of type II. It appears to be the non-local approximation which gives most of this effect.

Similar calculations were tried at the other two energies and for the type I potentials, but the lowest energy n_0 group was the only one that showed improvement.

The main failing of the type I calculations seems to be that they considerably overestimate the back angle cross sections. This effect seems to be caused by too much contribution from the nuclear interior. Rawitscher and Mukherjee[25] have found that in $^{40}Ca(d,p)$ at least, the main difference between a coupled channel calculation and a conventional DWBA calculation is that the contribution to the reaction from the nuclear interior is considerably damped in the coupled channel case. Meier et al.[11] have pointed out that this effect can be simulated in the DWBA analysis in a smooth manner by making the non-local parameters abnormally large. Calculations were tried at the two higher energies for type I potentials with the non-local parameters increased by a factor of three. The results are shown by the dot-dashed curves in Fig. 10. As might be expected, the cross sections at back angles drop considerably and have a more pronounced structure. These results may be an indication that a coupled channel analysis would yield better results.

Because of the poor description of the data using the DWBA model, the spectroscopic factors should be viewed with caution. They were obtained by normalizing the present cross section data to the data of Almond and Risser,[17] and comparing the calculated cross sections to the data at 20° (lab) according to the formula

$$S = \frac{1}{1.53\, C^2 \left(T_o \tfrac{1}{2}\, T_{o_3} \tfrac{-1}{2} \mid T_f\, T_{f_3}\right)} \cdot \frac{(2J_o+1)}{(2J_f+1)} (2j_{tr}+1) \frac{\sigma_{exp}}{\sigma_{calc}} .$$

The target and final state spins are denoted by J_0 and J_f, and the target and final state isotopic spins by T_0 and T_f. The total angular momentum transfer is j_{tr}. The spectroscopic factors for the finite range, non-local calculations of types I and II are listed in Table 5. The subscripts I and II in the table refer to the deuteron potential family. The factors for the n_1 reaction assume no $p_{3/2}$ component. No values are given for the results using the abnormally large non-local parameters as the interpretation of these calculations is unclear.

Table 5. The $^{11}B(d,n)$ Spectroscopic Factors.

	7.5 MeV		9.6 MeV		11.7 MeV		Cohen and Kurath[8]
	S_I	S_{II}	S_I	S_{II}	S_I	S_{II}	S
$^{11}B(d,n_0)$ $j_{tr} = 3/2$	2.3	2.3	4.0	7.1	3.3	6.5	5.7
$^{11}B(d,n_1)$ $j_{tr} = 1/2$	0.69	0.78	0.48	0.81	0.63	0.85	1.1

The predictions of Cohen and Kurath[8] are also shown in the table. The spectroscopic factors obtained from the calculations with type II parameters agree better with the theoretical ones, but considering the accuracy of the data and the quality of the agreement of the calculations with the data this is probably not significant.

It has been suggested by Meier et al.[11] that some of the anomalies associated with these reactions may be ascribed to the high Q values. Figure 11 shows a plot of the radial matrix elements for the $^{11}B(d,n_0)$ reaction for the 7.5b potential and a deuteron energy of 4 MeV. Compared with this plot is a similar plot for $^{14}N(d,n_0)$ by Meier et al.[11] with their 34-101.8-14.1 potential, a type II potential also. The $^{14}N(d,n_0)$ Q value is 5.07 MeV, while the $^{11}B(d,n_0)$ Q value is 13.7 MeV. The plots give an indication of the dominant ℓ-values for the reactions. The higher Q-value reaction ($^{11}B(d,n_0)$) has a wider range of ℓ-values contributing and might therefore be expected to behave differently from lower Q-value reactions.

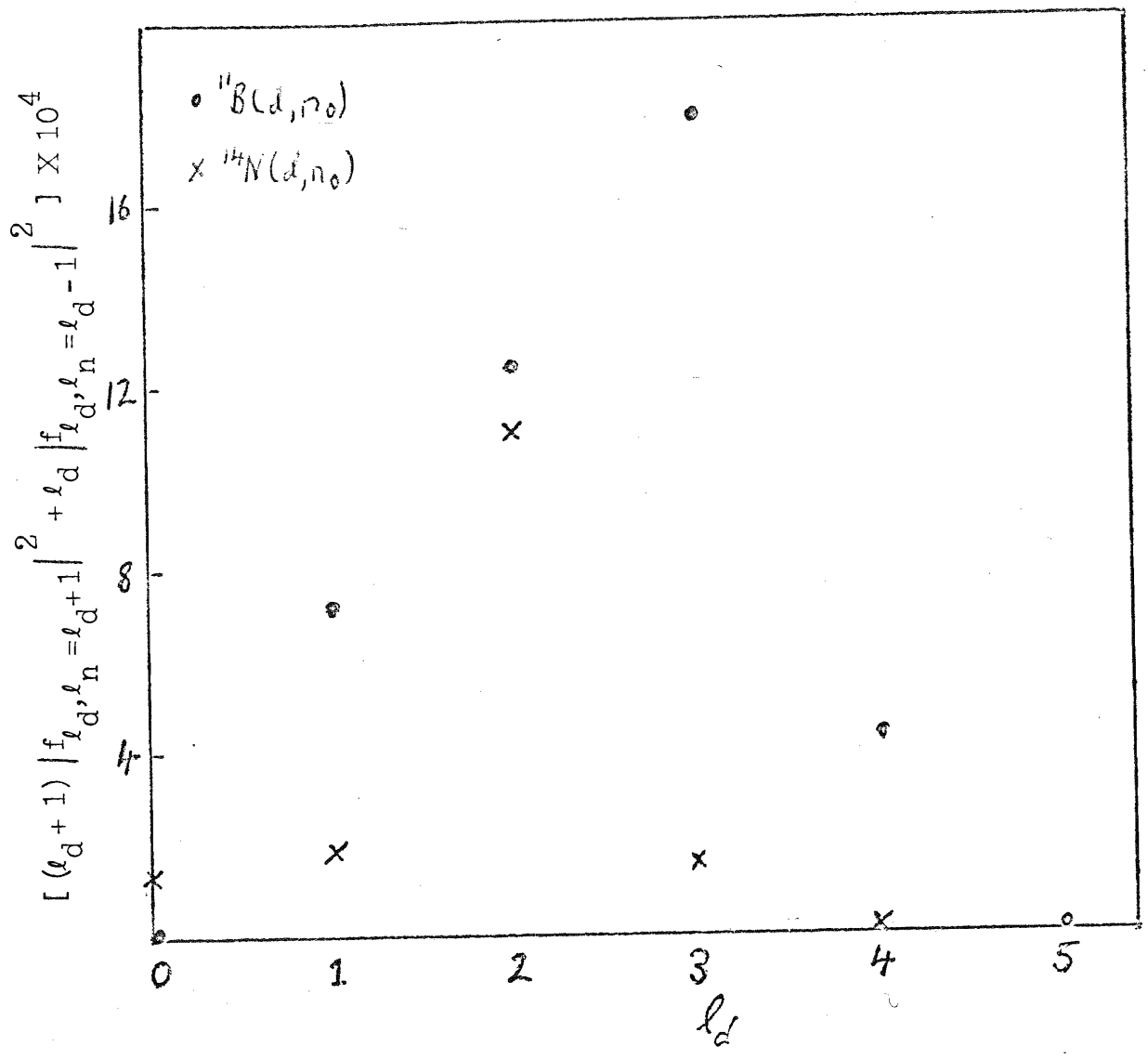

Figure 11. Radial Matrix Elements for $^{11}B(d,n_0)$ and $^{14}N(d,n_0)$. The ^{14}N data are from Ref. 11.

Chapter IV

THE $^{28}Si(d,n)^{29}P$ REACTIONS

A. Introduction

Deuteron induced reactions on ^{28}Si have been the subject of several analyses in the past few years. The DWBA theory has been used with some success to predict the general features of the $^{28}Si(d,n)$ reaction and its mirror reaction $^{28}Si(d,p)$. These reactions provide fairly stringent tests of stripping theories because the ground state of the target nucleus is a 0^+ and hence no mixtures of different total and orbital angular momentum transfers are allowed. In particular, both the $^{28}Si(d,n_0)$ and $^{28}Si(d,p_0)$ reactions proceed via $s_{1/2}$ transfers of the stripped particle, and the $^{28}Si(d,n_1)$ and $^{28}Si(d,p_1)$ reactions proceed by $d_{3/2}$ transfers.

There is a wealth of data on $^{28}Si+d$, and optical model parameters for the input channel should be fairly well determined. There exists elastic cross section data from 1 to 15 MeV,[26-33,10] and tensor polarizations have been measured at 9 MeV.[29] The $^{28}Si(d,p)$ differential cross sections have been measured at several energies in this range.[28,34-39] Proton polariza-

tions for this reaction have been investigated at five energies.[28,39-42] Cross sections for the (d,n) reactions are available from 2.7 to 9 MeV,[43-46] and the (d,n) neutron polarization was reported at 5 MeV.[47] The present measurements complement this neutron polarization measurement by providing polarization angular distributions between 3 and 4 MeV and at 8 MeV.

B. Experiment

The ^{28}Si(d,n) measurements were performed in two phases. Data below 4 MeV were taken on the TUNL 4 MeV Van de Graaff accelerator, and measurements at 8 MeV were made using the TUNL tandem Van de Graaff. The experimental configurations were different for these two phases and hence are discussed separately.

Targets for the low energy data were made by evaporating natural silicon metal onto tantalum endcaps with an electron gun. The average energy loss of the deuteron beam in the target was about 120 keV at 3.5 MeV. Two NE-213 liquid scintillators (5.08 X 7.62 X 15.3 cm^3) were used as 120° side detectors and were placed 24 cm (center-to-center) from the helium scintillator, which was pressurized to 115 atm. The spin precession solenoid was operated at a current which could precess a 1.51 MeV neutron through 90°. Four polarization angular distributions for the ^{28}Si(d,n$_0$) group were taken at mean deuteron energies of 2.95, 3.25, 3.55, and 3.85 MeV. Polarization excitation functions were obtained from 2.95 to 3.85 MeV at

20° (lab) and 40° (lab). Carbon contamination prevented extraction of data for the n_1 neutron group. The resolution of the gated He-recoil peak was about 19% (FWHM), and this was too high to separate the $^{28}Si(d,n_1)$ and $^{12}C(d,n_0)$ neutron groups. Likewise, the n_2 group was obscured by neutrons from the $^{16}O(d,n)$ reactions.

The measurements at 8 MeV were made using a more satisfactory target arrangement than at the lower energies. The target was a 38 micron silicon wafer which was etched from a 150 micron detector blank in the following manner. The silicon crystal was first cleaned in a strong detergent, hot toluene, and then in a glass cleaning solution consisting of 35 parts sodium dichromate solution to 1000 parts sulfuric acid. The cleaning was continued until the surface wet uniformly in distilled water. The wafer was then embedded in a small paraffin block with only the central part of one face exposed. The purpose of this was to keep the edges from being rapidly eaten away during the etching process. The block and wafer were then immersed in an etching solution of 10 parts nitric acid to 1 part hydroflouric acid. After several minutes the etching solution was diluted and the block removed and rinsed. The solution must be diluted or the crystal will tarnish upon contact with the air. The paraffin was dissolved in hot toluene and the crystal was measured to within 3 microns. The whole process was repeated until an acceptable thickness was reached. The wafer was mounted inside a stainless steel tube (wall thickness 250 microns). The beam was stopped in a tantalum endcap mounted 7.6 cm beyond the wafer. This was far enough

away from the target so that neutrons originating from the endcap could not be seen directly by the detectors. The target presented an energy loss of 650 keV to the incident deuteron beam, and the mean deuteron energy was 8.1 MeV.

Two plastic Ne102 scintillators (5.08 X 7.62 X 15.3 cm^3) served as side detectors and were mounted at a scattering angle $\theta_2 = 120^o$ and at a distance of 24 cm (center to center) from the helium cell. Two helium cells were used during the course of the measurements. Both were pressurized to 140 atm with a mixture of 5% xenon and 95% helium. The first had a gated He-recoil peak resolution of 12%, the second, 15%. The better resolution was sufficient to allow extraction of data for the n_1 group along with the n_0, but data points for the n_1 group using the second cell are not reported. Data for the n_2 group are also not reported because of uncertainties due to the closeness of the n_3 and n_1 groups and neutrons from the $^{16}O(d,n)$ reaction due to oxygen at the target surface. The solenoid was operated at a current that precessed the polarization of a 7.7 MeV neutron beam through 90^o.

All of the data were analyzed by fitting the spectra with Gaussian peaks using the programs described in chapter II. The resolution parameters were searched on at a few angles where the n_0 group stood out clearly and were fixed for the rest of the data. Figure 12 shows a typical summed spectrum and its decomposition into Gaussian peaks. The rightmost group corresponds to neutrons from the $^{28}Si(d,n_0)$ reaction and the next one to the $^{28}Si(d,n_1)$ reaction.

Figure 12. Typical Summed Spectrum and Fit for $^{28}Si(d,n)$.

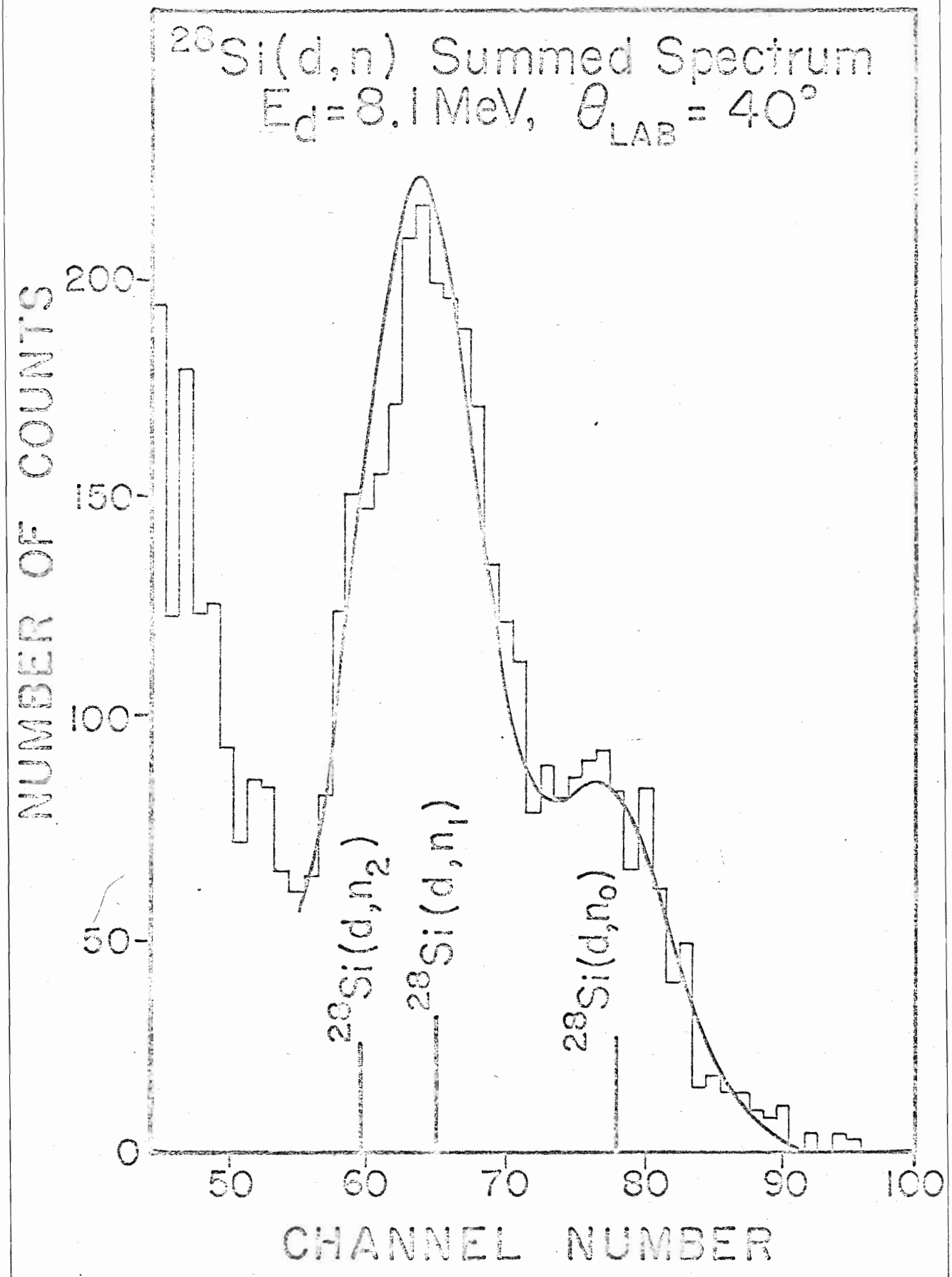
^{28}Si(d,n) Summed Spectrum
E_d = 8.1 MeV, θ_{LAB} = 40°
NUMBER OF COUNTS
0
50
100
150
200
50
60
70
80
90
100
CHANNEL NUMBER
^{28}Si(d,n$_2$)
^{28}Si(d,n$_1$)
^{28}Si(d,n$_0$)

C. Results and Comparison With Other Data

The polarization angular distributions from 2.84 to 3.84 MeV are shown in Fig. 13 and are tabulated in Table 6. Their diversity indicates that compound nucleus effects are probably quite important at these energies. With the exception of the lowest energy, however, the negative polarization in the region of 40° (c.m.) is fairly persistent. The polarization excitation functions at 20° and 40° (lab) are shown in Fig. 14. Again fluctuations are quite evident. The data are also listed in Table 6.

The data at 8.1 MeV are listed in Table 7 and are compared in Fig. 15 with the data of Lam et al.[47] at 5 MeV. The data for the two energies are quite similar, indicating that compound nucleus effects are probably well averaged out for this data, if they are contributing at all. The excitation energy in the compound nucleus is nearly 20 MeV, so that the mean level spacing should be quite small in comparison to the target thickness. The main effect of such a compound nucleus contribution on the polarization would be to dilute it by the percentage of the contribution.

D. DWBA Calculations and Conclusions

There have been three recent optical model analyses which should be considered as a source of deuteron parameters for the DWBA study. Schwandt and Haeberli[29] analyzed the elastic cross section and polarization

Figure 13. The $^{28}Si(d,n_0)$ Polarization Distributions from 2.9 to 3.8 MeV.

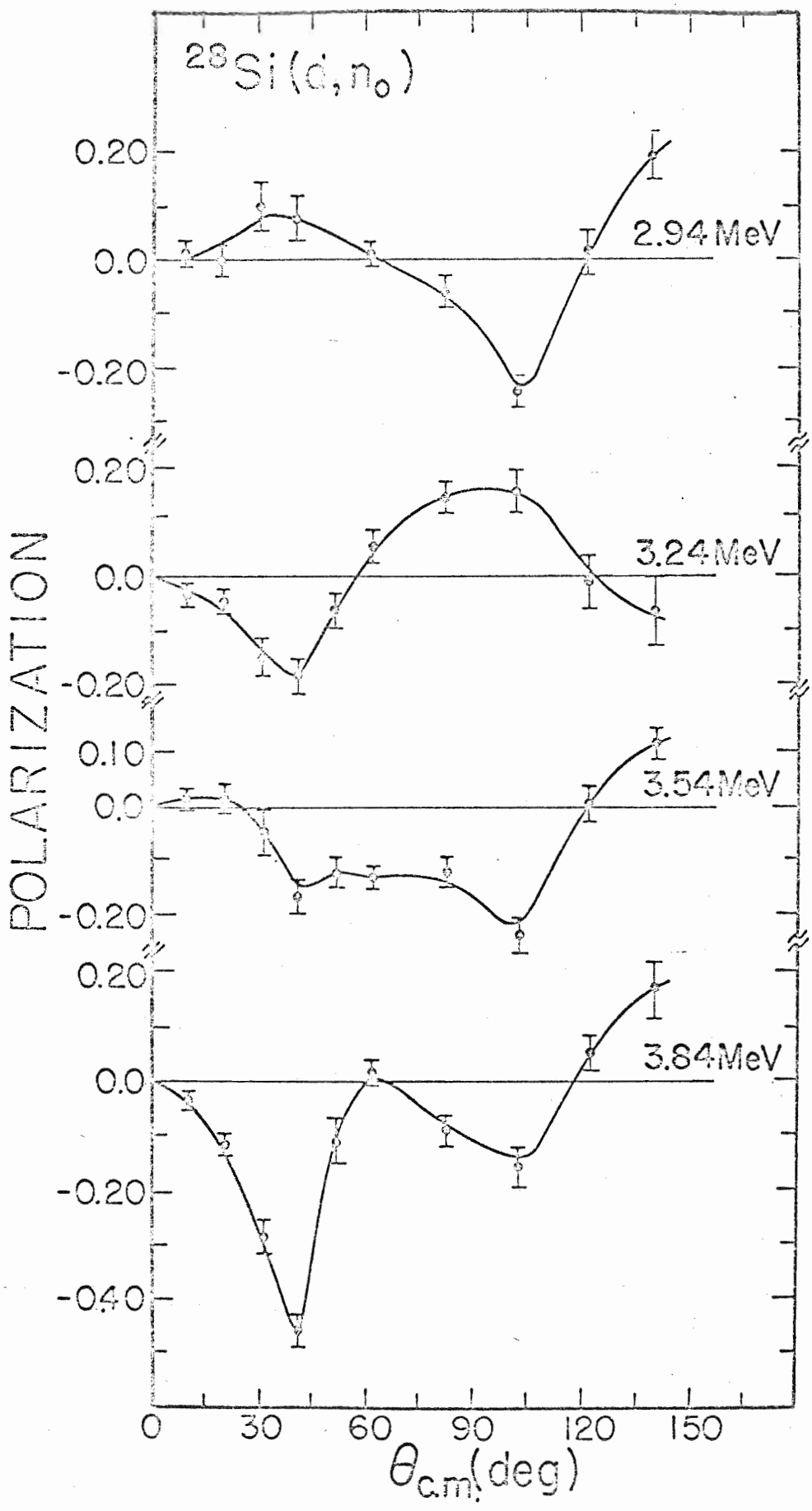
$^{28}Si(d,n_0)$
2.94 MeV
3.24 MeV
3.54 MeV
3.84 MeV
POLARIZATION
0.20
0.0
-0.20
0.10
-0.40
0
30
60
90
120
150
$\theta_{c.m.}$(deg)

Table 6. $^{28}Si(d,n_0)$ Polarization Angular Distributions and Excitation Functions below 4 MeV.

E_d (MeV)	θ_{lab} (deg)	$\theta_{C.M.}$ (deg)	Asymmetry	SPF	$\overline{P_2}$	Polarization
2.95	10	10.5	0.010 ± 0.019	1.17	0.94	0.012 ± 0.024
	20	20.9	-0.002 ± 0.022	1.17	0.94	-0.002 ± 0.027
	30	31.3	0.080 ± 0.035	1.17	0.94	0.099 ± 0.043
	40	41.7	0.057 ± 0.032	1.16	0.93	0.071 ± 0.040
	60	62.3	0.005 ± 0.017	1.15	0.93	0.006 ± 0.021
	80	82.6	-0.048 ± 0.019	1.14	0.92	-0.060 ± 0.024
	100	102.6	-0.200 ± 0.024	1.13	0.91	-0.248 ± 0.030
	120	122.3	0.006 ± 0.035	1.13	0.91	0.007 ± 0.042
	140	141.7	0.152 ± 0.035	1.12	0.90	0.188 ± 0.043
3.25	10	10.5	-0.026 ± 0.015	1.18	0.94	-0.032 ± 0.019
	20	20.9	-0.037 ± 0.016	1.18	0.94	-0.046 ± 0.020
	30	31.3	-0.118 ± 0.024	1.17	0.94	-0.148 ± 0.030
	40	41.7	-0.145 ± 0.025	1.17	0.94	-0.182 ± 0.031
	50	52.0	-0.052 ± 0.024	1.17	0.94	-0.065 ± 0.030
	60	62.3	0.041 ± 0.022	1.17	0.94	0.051 ± 0.028
	80	82.6	0.111 ± 0.022	1.17	0.94	0.139 ± 0.028
	100	102.6	0.119 ± 0.028	1.16	0.93	0.149 ± 0.035
	120	122.3	-0.012 ± 0.038	1.14	0.92	-0.015 ± 0.048
	140	141.7	-0.053 ± 0.049	1.12	0.90	-0.068 ± 0.061
3.55	10	10.5	0.010 ± 0.012	1.22	0.94	0.013 ± 0.016
	20	20.9	0.012 ± 0.019	1.22	0.94	0.016 ± 0.025
	30	31.3	-0.034 ± 0.032	1.21	0.94	-0.044 ± 0.041
	40	41.7	-0.128 ± 0.022	1.28	0.94	-0.164 ± 0.028
	50	52.0	-0.094 ± 0.018	1.28	0.94	-0.120 ± 0.023
	60	62.3	-0.102 ± 0.016	1.19	0.94	-0.130 ± 0.020
	80	82.6	-0.097 ± 0.019	1.17	0.94	-0.121 ± 0.024
	100	102.6	-0.190 ± 0.023	1.16	0.94	-0.236 ± 0.029
	120	122.3	0.004 ± 0.023	1.16	0.94	0.005 ± 0.028
	140	141.7	0.090 ± 0.023	1.16	0.94	0.112 ± 0.028

Table 6. (continued)

E_d (MeV)	θ_{lab} (deg)	$\theta_{C.M.}$ (deg)	Asymmetry	SPF	$\overline{P_2}$	Polarization
3.85	10	10.5	-0.026 ± 0.010	1.24	0.94	-0.035 ± 0.013
	20	20.9	-0.088 ± 0.013	1.23	0.94	-0.115 ± 0.017
	30	31.3	-0.218 ± 0.023	1.23	0.94	-0.286 ± 0.030
	40	41.2	-0.352 ± 0.023	1.23	0.94	-0.460 ± 0.030
	50	52.1	-0.082 ± 0.030	1.23	0.94	-0.107 ± 0.039
	60	62.3	0.014 ± 0.017	1.20	0.94	0.018 ± 0.022
	80	82.6	-0.069 ± 0.020	1.21	0.94	-0.089 ± 0.026
	100	102.6	-0.125 ± 0.030	1.19	0.94	-0.158 ± 0.038
	120	122.3	0.042 ± 0.026	1.18	0.94	0.052 ± 0.032
	140	141.7	0.133 ± 0.040	1.16	0.94	0.164 ± 0.049
2.75	20		-0.039 ± 0.041	1.15	0.93	-0.048 ± 0.051
2.85	20		-0.082 ± 0.027	1.16	0.94	-0.102 ± 0.033
3.05	20		0.019 ± 0.025	1.16	0.94	0.024 ± 0.031
3.15	20		-0.116 ± 0.040	1.17	0.94	-0.145 ± 0.050
3.35	20		0.034 ± 0.018	1.20	0.94	0.044 ± 0.023
3.45	20		-0.005 ± 0.019	1.22	0.94	-0.006 ± 0.025
3.65	20		0.023 ± 0.028	1.24	0.94	0.030 ± 0.036
3.75	20		-0.051 ± 0.017	1.25	0.94	-0.066 ± 0.022
2.75	40		-0.075 ± 0.045	1.14	0.92	-0.093 ± 0.056
2.85	40		0.061 ± 0.032	1.15	0.93	0.076 ± 0.040
3.05	40		0.082 ± 0.037	1.16	0.94	0.102 ± 0.046
3.15	40		-0.013 ± 0.029	1.16	0.94	-0.016 ± 0.036
3.35	40		-0.125 ± 0.031	1.18	0.94	-0.158 ± 0.039
3.45	40		-0.225 ± 0.030	1.16	0.94	-0.285 ± 0.038
3.65	40		-0.101 ± 0.024	1.23	0.94	-0.132 ± 0.031
3.70	40		-0.278 ± 0.022	1.24	0.94	-0.367 ± 0.029
3.75	40		-0.395 ± 0.026	1.24	0.94	-0.521 ± 0.034

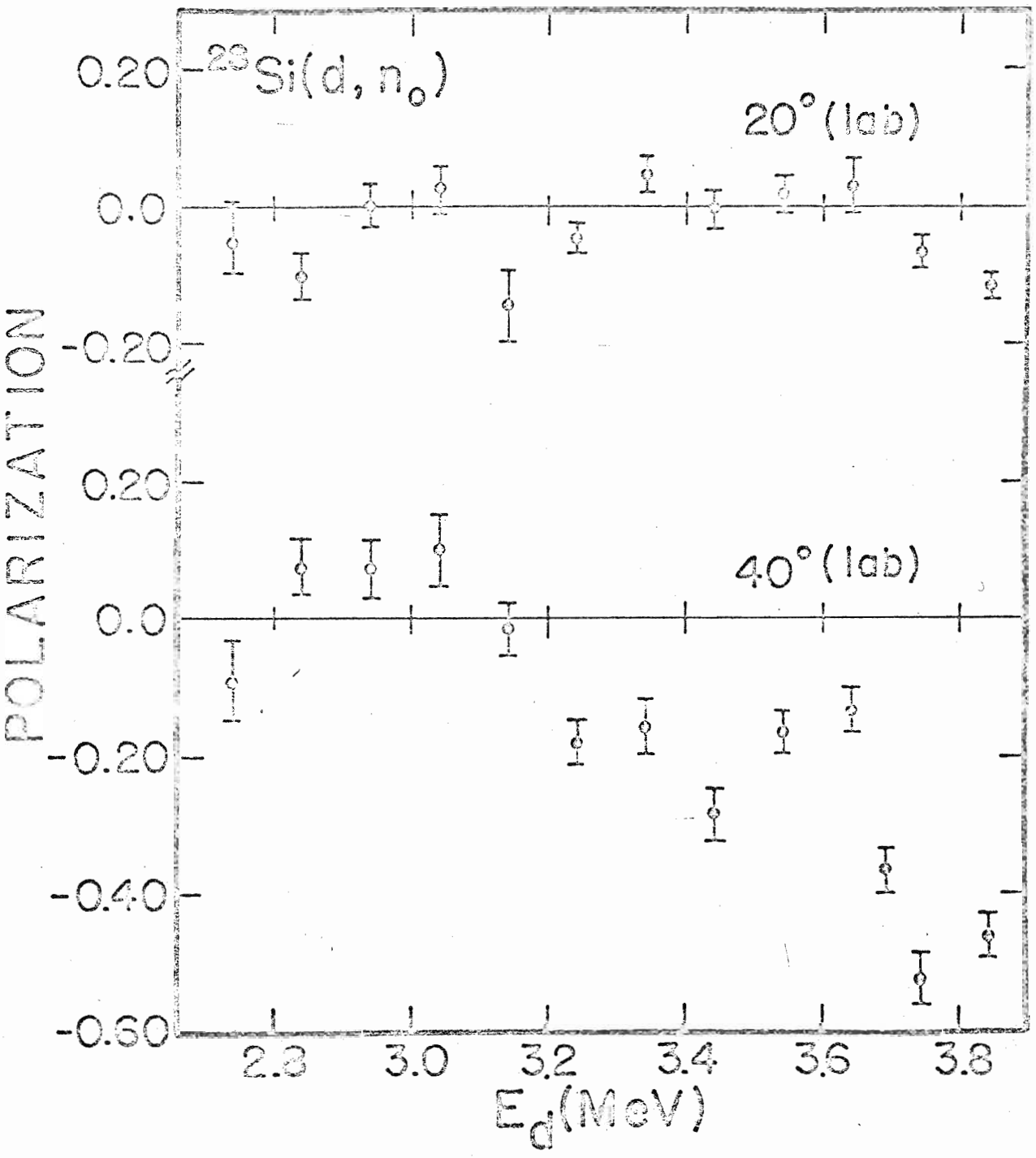

Figure 14. The $^{28}Si(d, n_0)$ Polarization at 20° and 40° (lab from 2.75 to 3.75 MeV.

Table 7. Polarizations for the ^{28}Si(d,n) Reactions at 8.1 MeV.

Reaction	θ_{lab} (deg)	$\theta_{c.m.}$ (deg)	Asymmetry	$\overline{P_2}$	Polarization
^{28}Si(d,n$_0$)	5	5.2	0.000 ± 0.013	0.92	0.000 ± 0.014
	10	10.5	-0.024 ± 0.017	0.92	-0.026 ± 0.018
	15	15.7	-0.012 ± 0.012	0.92	-0.013 ± 0.013
	20	21.0	-0.041 ± 0.019	0.92	-0.044 ± 0.020
	25	26.2	-0.157 ± 0.028	0.92	-0.171 ± 0.030
	30	31.4	-0.064 ± 0.048	0.92	-0.069 ± 0.053
	35	36.6	-0.008 ± 0.043	0.92	-0.008 ± 0.046
	40	41.8	0.079 ± 0.037	0.92	0.086 ± 0.040
	50	52.1	0.155 ± 0.029	0.92	0.168 ± 0.032
	60	62.4	0.206 ± 0.050	0.92	0.235 ± 0.054
	65	67.5	0.222 ± 0.049	0.92	0.243 ± 0.053
	70	72.6	-0.025 ± 0.043	0.92	-0.027 ± 0.046
	75	77.7	-0.131 ± 0.047	0.92	-0.142 ± 0.051
	85	87.8	-0.117 ± 0.051	0.92	-0.127 ± 0.055
	95	97.8	0.025 ± 0.071	0.92	0.027 ± 0.077
	110	112.6	0.126 ± 0.071	0.92	0.137 ± 0.077
	120	122.4	0.122 ± 0.058	0.92	0.133 ± 0.063
^{28}Si(d,n$_1$)	5	5.3	0.088 ± 0.066	0.93	0.094 ± 0.072
	10	10.5	0.057 ± 0.059	0.93	0.061 ± 0.063
	15	15.8	-0.009 ± 0.040	0.93	-0.009 ± 0.043
	20	21.0	0.030 ± 0.033	0.93	0.032 ± 0.035
	25	26.3	-0.024 ± 0.016	0.93	-0.025 ± 0.017
	30	31.5	-0.030 ± 0.017	0.93	-0.032 ± 0.019
	35	36.8	-0.065 ± 0.024	0.93	-0.070 ± 0.025
	40	42.8	-0.084 ± 0.028	0.93	-0.090 ± 0.030
	50	52.3	-0.134 ± 0.050	0.93	-0.144 ± 0.054
	60	62.7	-0.177 ± 0.064	0.93	-0.190 ± 0.069

Figure 15. The $^{28}Si(d,n_0)$ and $^{28}Si(d,n_1)$ Polarization Distributions at 8.1 MeV. The data at 5.1 MeV are from Ref. 47. The solid lines are from DWBA calculations.

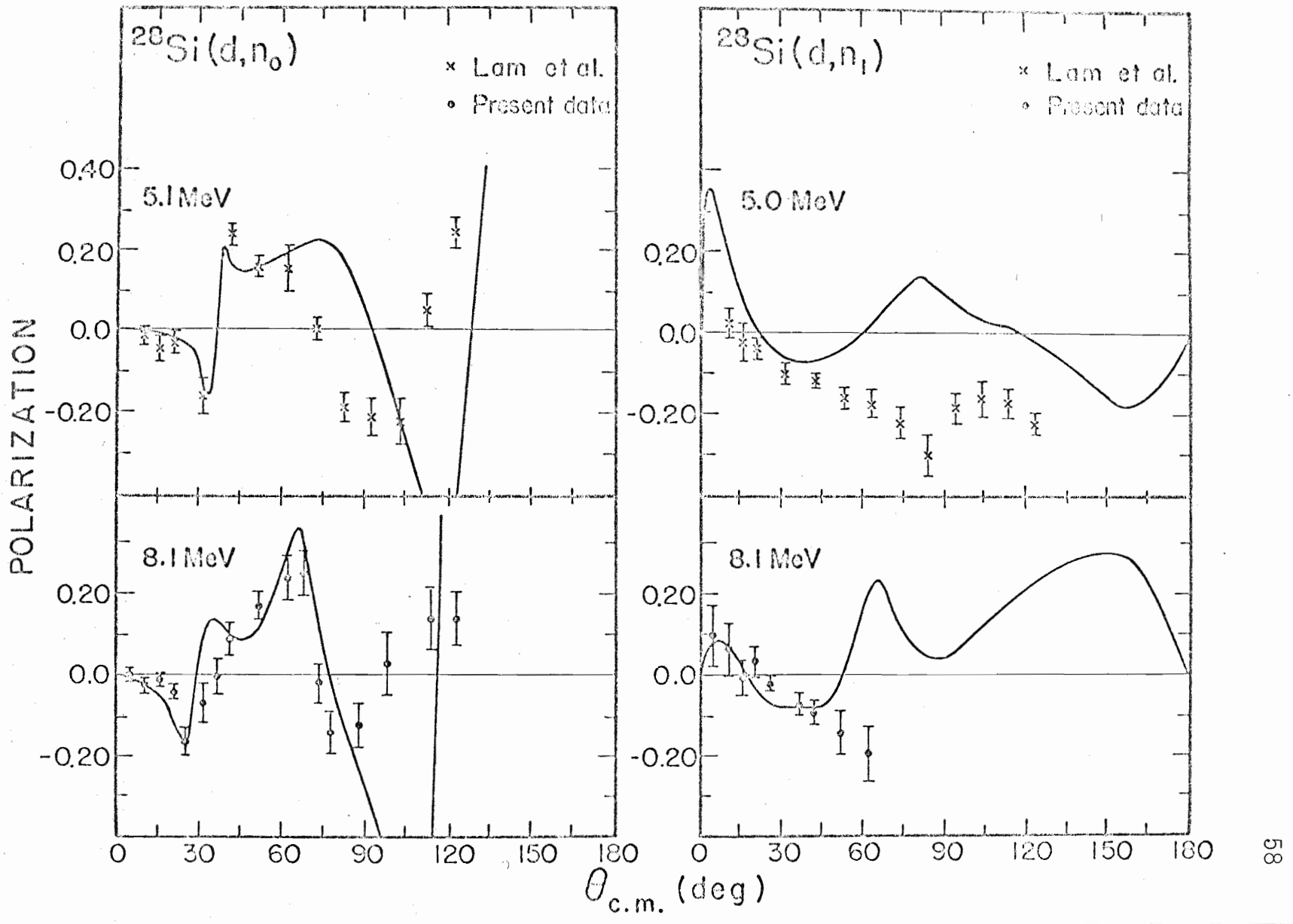
$^{28}Si(d,n_0)$
× Lam et al.
∘ Present data
5.1 MeV
8.1 MeV
$^{28}Si(d,n_1)$
× Lam et al.
∘ Present data
5.0 MeV
8.1 MeV
POLARIZATION
0.40
0.20
0.0
-0.20
0
30
60
90
120
150
180
$\theta_{c.m.}$ (deg)

data at 9 MeV. The real well depth was kept close to 100 MeV and the radius r_0 was constrained between 1.0 and 1.1 fm. They obtained quite good agreement with the differential cross section data, but only fair agreement with the polarization data. Gurd et al.[28] analyzed elastic cross section data around 5 MeV and found three discrete parameter families characterized by values of V and r_0 of (55, 1.4), (106, 1.18), and (158, 1.22). The third analysis was performed by Lacek and Strohbusch[27] on data between 5.1 and 12 MeV. They also found three parameter families which correspond roughly to those of Gurd. In the present work it was decided to use the parameters of Lacek and Strohbusch because their parameters represented the data over a wider energy range. Only the middle set was used because the work of Gurd and a separate (d,p) analysis by Strohbusch et al.[35] showed that only parameters corresponding to the middle set would produce reasonable results for the (d,p) reactions. The energy dependence of this parameter set is shown in Table 8 where E is the lab deuteron energy. The major problem with the set was that it did not contain a spin-orbit term, as the elastic scattering was insensitive to its inclusion. For the present work a spin-orbit potential of V_{so} = 6 MeV, r_{so} = 1.2, and a_{so} = 0.65 was included. This term is similar to the 7 MeV spin-orbit potential of Schwandt and Haeberli.[29] DWBA calculations showed that the reaction results were reasonably insensitive to the magnitude of this term.

Table 8. The Deuteron Potential Set of Lacek et al.[27]

$V = 109.5 - 1.25\ E$	$W_d = -2.11 + 2.51\ E$
$r_0 = 1.283 - 0.012\ E$	$r_i = 1.394 + 0.012\ E$
$a_0 = 0.501 + 0.032\ E$	$a_i = 0.828 - 0.029\ E$

Because of the strong fluctuations in the lower energy data, it was decided to confine the DWBA analysis to the 8.1 MeV data. In addition, checks were made on existing data above 5 MeV. Optical model parameters for the outgoing neutron channel were taken from Perey and Buck.[49] Figure 15 shows the results of the DWBA polarization calculations at 5 and 8 MeV. The 5 MeV calculation describes the data of Lam about as well as the potential set of Gurd. The DWBA calculation for the n_1 group still misses the experimental polarization badly. The calculation at 8 MeV for the n_0 group describes the measured data reasonably well for angles less than 90° (c.m.), but the n_1 calculation again misses the experimental data. Shown in Fig. 16 are the differential cross section calculations at 5 and 7 MeV compared with the data of Davies et al.[44] and Buccino et al.,[45] respectively. The predictions are reasonable considering that compound reaction contributions have not been taken into account. Spectroscopic factors for these calculations are presented in Table 9. Relative spectroscopic factors are in parentheses. Also listed are the spectroscopic factors from Lam et al.[47] for the same

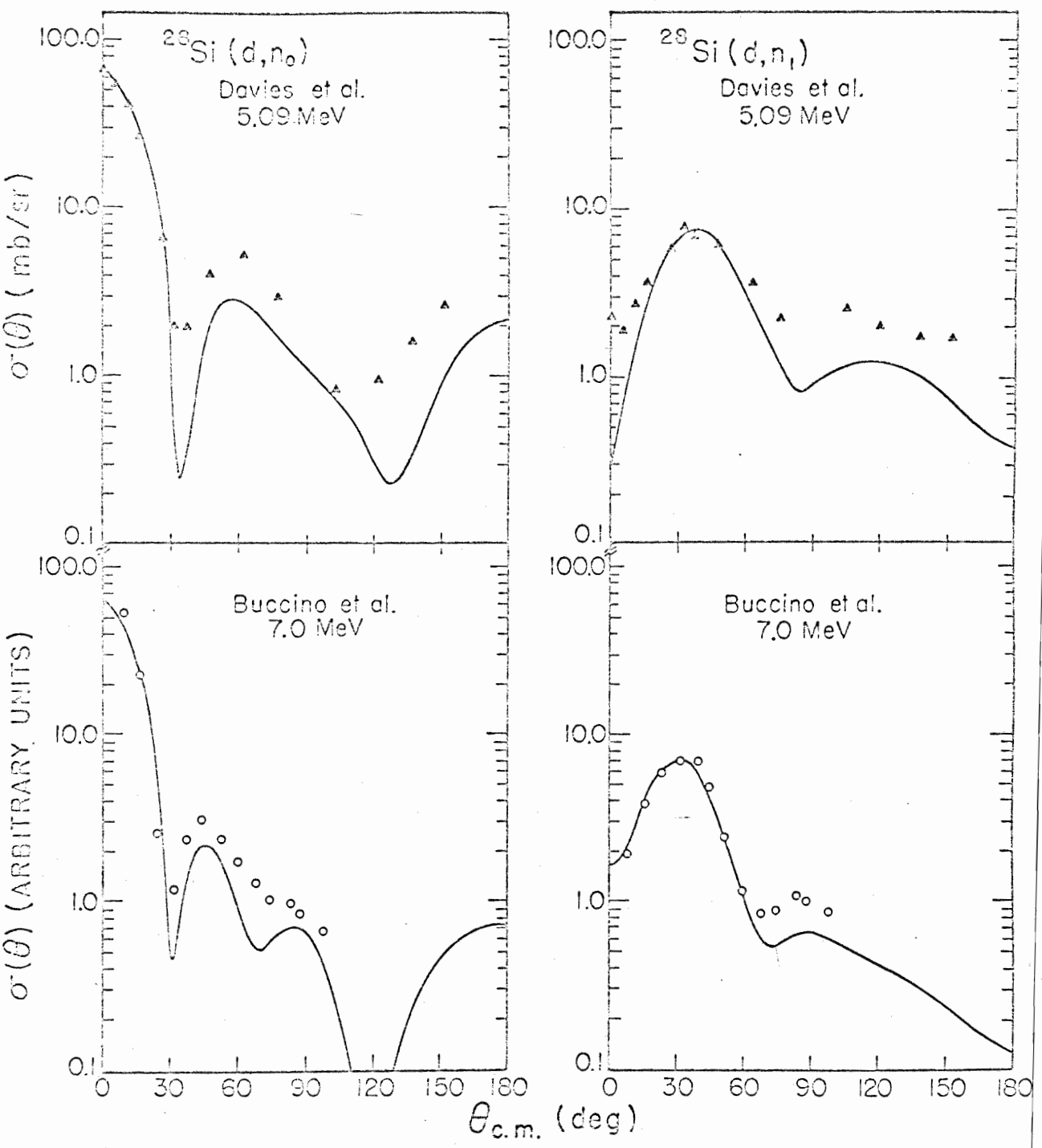

Figure 16. DWBA Cross Section Calculations for ^{28}Si(d,n$_0$) and ^{28}Si(d,n$_1$). The data are from Ref. 44 and Ref. 45.

data at 5 MeV, from the ^{28}Si(d,p) work of Glower[50] at 10 MeV, and from the (d,p) work of Strohbusch et al.[35] below 6 MeV. The results of a Nilsson model calculation by Davies et al.[44] are also presented.

Table 9. Spectroscopic Factors for ^{28}Si(d,n) and ^{28}Si(d,p)

	S ground state		S 1st excited state	
7.0 MeV (d,n) data of Buccino		(1.0)		(1.55)
5.0 MeV (d,n) data of Davies	0.42	(1.0)	0.69	(1.64)
5.0 MeV (d,n) Lam claculations on data of Davies	0.37	(1.0)	0.59	(1.6)
10.0 MeV (d,p) work of Glower	0.51	(1.0)	0.82	(2.2)
4.5 - 5.8 MeV (d,p) work of Strohbusch	0.54	(1.0)	1.0	(1.9)
Nilsson model calculations of Davies		(1.0)		(2.1)

It is also interesting to compare the (d,p) polarization data to DWBA calculations which use the potential set listed in Table 8. Figure 17 shows the ^{28}Si(d,p) polarization data of Bercaw and Shull[40] at 10 MeV and Maddox, Kelley and Miller[41] at 10.8 MeV. The DWBA calculation was per-

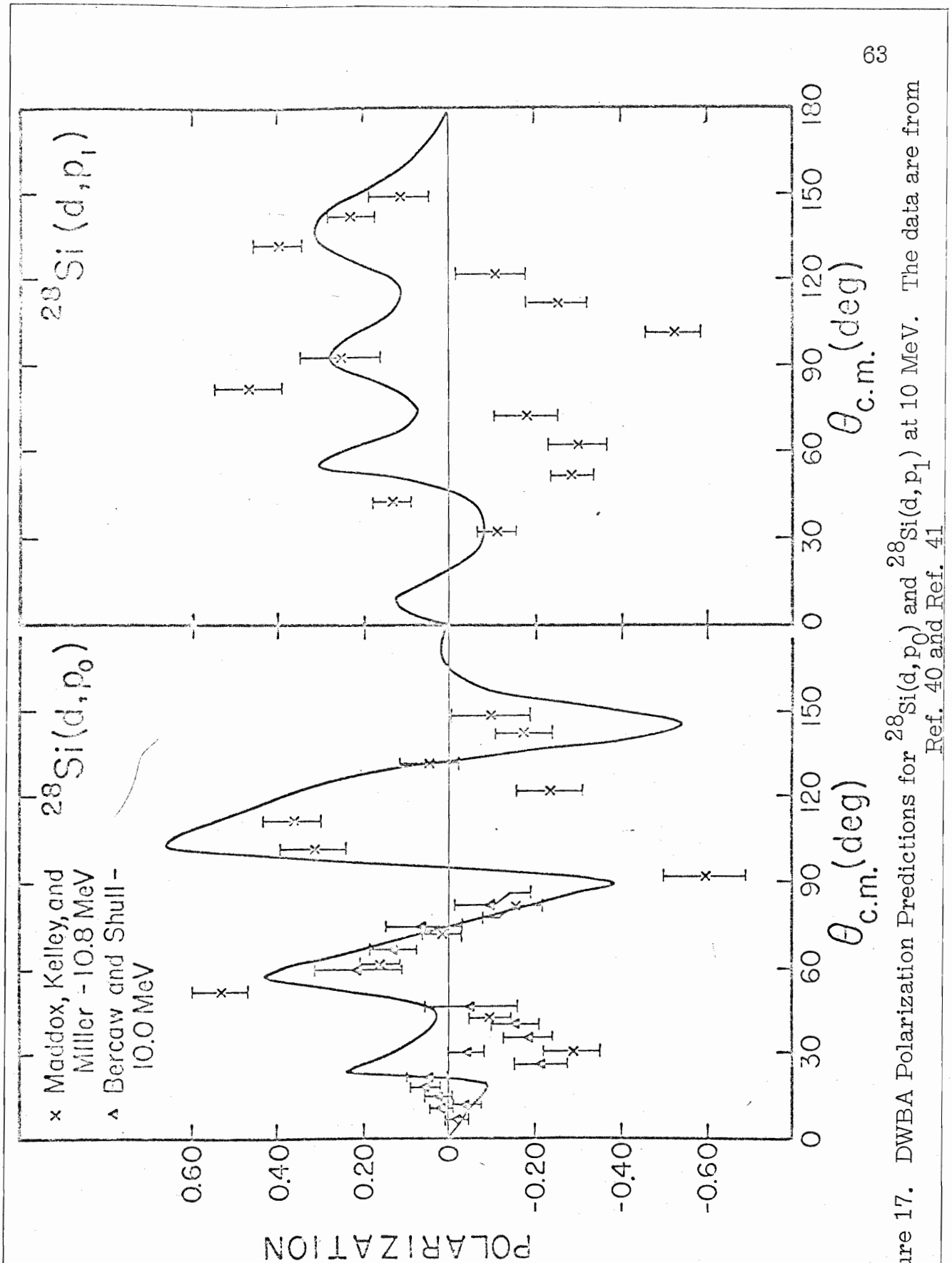

Figure 17. DWBA Polarization Predictions for ^{28}Si(d, p$_0$) and ^{28}Si(d, p$_1$) at 10 MeV. The data are from Ref. 40 and Ref. 41

formed at 10 MeV and does not fit the data. The proton parameters are from Perey.[25] It should be mentioned that the DWBA calculation of Goldfarb which was included in Fig. 12 of Ref. 41 was a fit at 15 MeV to the data of Isoya and Marrone[39] and not a fit to the 10 MeV data of Bercaw and Shull,[40] as was indicated in the caption. This particular calculation gives an excellent fit to the polarization data at 15 MeV.

As far as polarization data is concerned, the DWBA theory appears to describe the (d,n_0) reaction fairly well, the (d,n_1) reaction poorly, and the (d,p_0) reaction not particularly well. The (d,p_1) calculations bear no resemblance whatsoever to the polarization data. All of the differential cross sections are described adequately, however. Part of the difficulties might be attributed to the well known fact that ^{28}Si is not a good closed shell nucleus. Perhaps the trouble with the first excited state calculations can be ascribed to a poor description of bound state wave functions.

Chapter V

THE ^{24}Mg(d,n) REACTIONS

A. Introduction

Another stripping reaction near the middle of the s-d shell is the ^{24}Mg(d,n) reaction. The (d,n_0) reaction, which leaves ^{25}Al in its $5/2^+$ ground state is a $d_{5/2}$ transfer. The ^{24}Mg(d,n_1) reaction proceeds via an $s_{1/2}$ transfer to the first excited state of ^{25}Al, which is a $1/2^+$ state. Polarization angular distributions for these two neutron groups were measured at six energies between 2 and 4 MeV, and polarization excitation functions were taken at two angles.

B. Experiment

Targets were made from enriched MgO in a reduction process. Tantalum powder was mixed with the MgO (99.96% ^{24}Mg) and the mixture was heated with an electron gun. The Mg metal was deposited onto tantalum endcaps. Target thicknesses ranged from 150 to 300 $\mu g/cm^2$. The experi-

mental arrangement was identical with that for the low energy Si(d,n) measurements. Data were extracted for both the n_0 and n_1 neutron groups. Because neutrons from the $^{12}C(d,n)$ reaction lie kinematically close to the n_1 group, checks were made for ^{12}C contaminants. Carbon sometimes builds up on targets where the beam strikes (presumably from CO_2), so checks were made where the carbon polarization was high before and after replacing a target. No evidence of appreciable contamination was found.

C. Results

Figure 18 shows the results of the polarization angular distributions at 2.2, 2.6, 3.0, 3.3, 3.6, and 3.9 MeV. The solid lines serve only to guide the eye and have no theoretical significance. The data are listed in Tables 10 and 11. Figure 19 shows the polarization excitation functions at 20° and 40° (lab). The $^{24}Mg(d,n_0)$ reaction exhibits quite diverse distributions — presumably from compound nucleus contributions. At most of the energies the polarization shows a negative polarization at forward angles. The $^{24}Mg(d,n_1)$ reaction also exhibits fluctuations over the region, but not as badly. With the exception of one energy, it shows the same strong negative polarization around 40° (c.m.) as was characteristic of the $^{28}Si(d,n_0)$ reaction at similar energies. Both are $\ell = 0$ transfers.

Dietzsch et al.[50] have investigated the behavior of the differential cross sections in this energy region. They performed Hauser-Feshbach

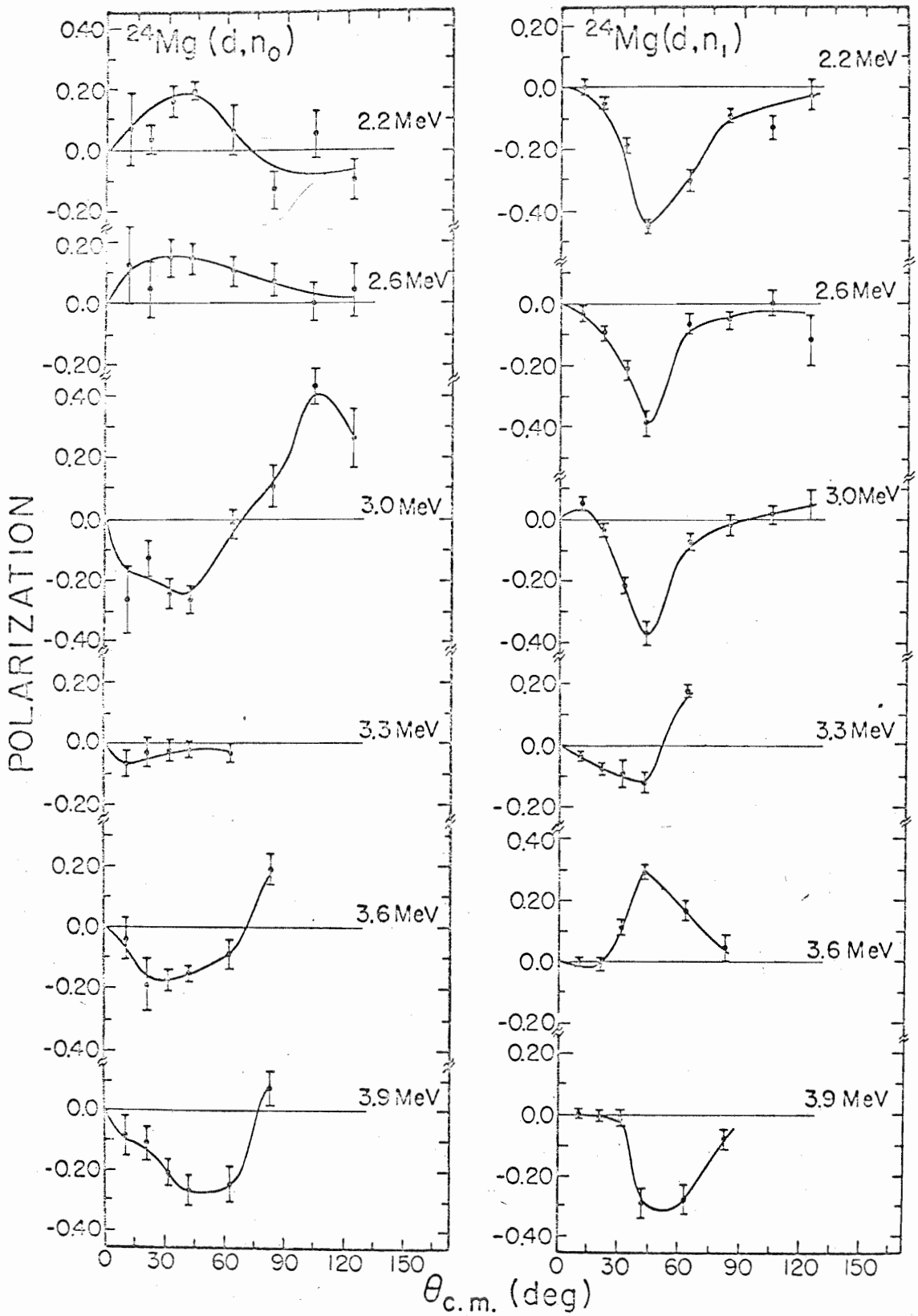

Figure 18. The ^{24}Mg(d, n$_0$) and ^{24}Mg(d, n$_1$) Polarization Angular Distributions.

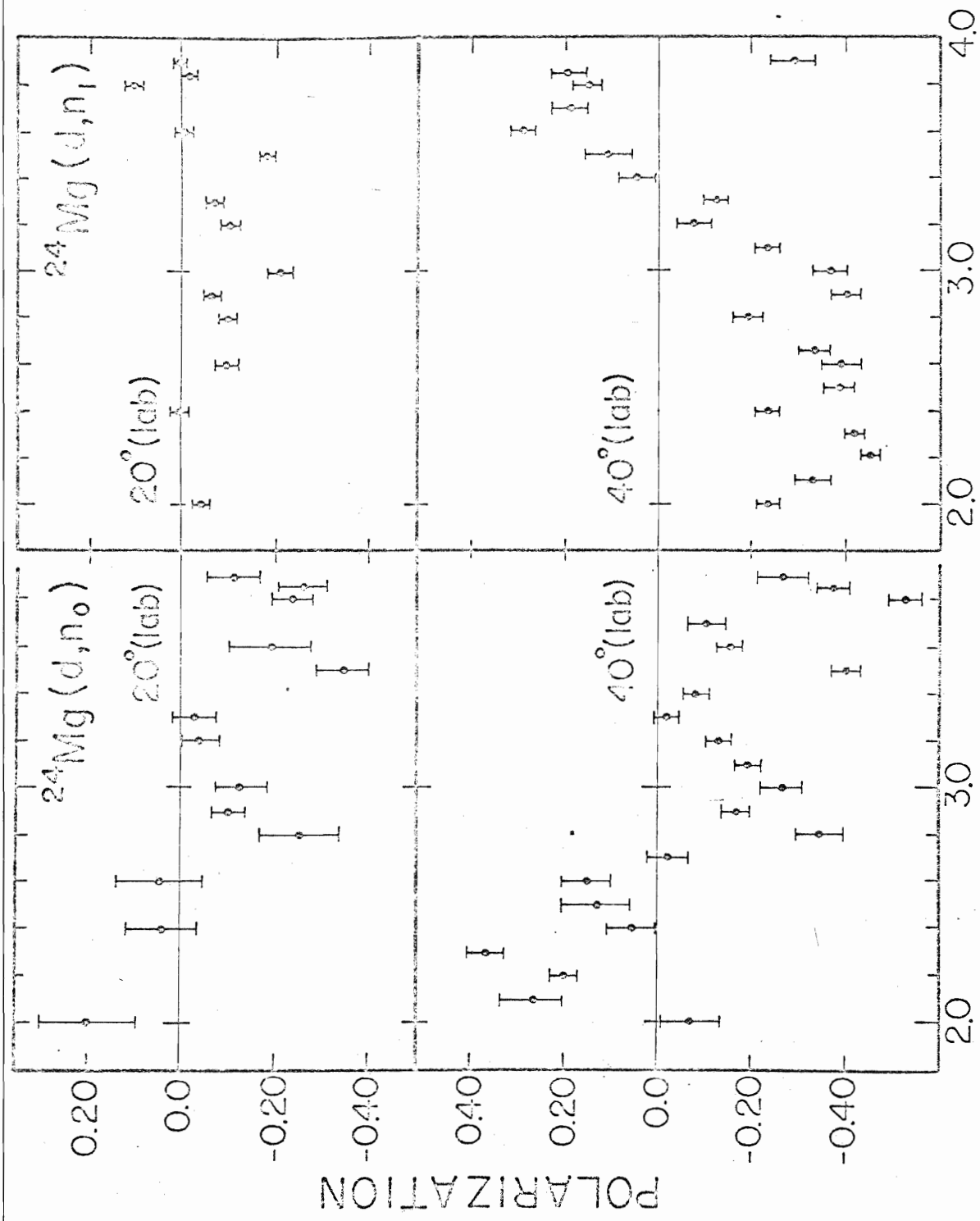

Figure 19. The $^{24}Mg(d,n_0)$ and $^{24}Mg(d,n_1)$ Polarization at 20° and 40° (lab).

calculations to estimate the amount of compound nucleus contribution in this reaction. For the n_0 group their calculation showed that the average contribution was greater than 25% at all angles, and at back angles was considerably larger than the direct contribution. It is not surprising that the n_0 polarization distributions are fluctuating with this large amount of compound nucleus contribution. Their Hauser-Feshbach calculations for the n_1 group showed that the relative amount of compound nucleus contribution was considerably smaller. This would tend to explain why the n_1 polarization distributions fluctuate less than the n_0. The position of the maximum polarization is also the position of the first minimum in the cross section, which means that this region is likely to be greatly influenced by compound nucleus formation. Because of the large fluctuations in both neutron groups, it was felt that DWBA calculations would not be of any significant value until more data at higher energy are available to demonstrate the energy dependence over a greater energy range. Our technique has resolution problems for this reaction above 4 MeV and such data would require time-of-flight separation of the neutron groups.

Table 10. The $^{24}Mg(d,n_0)$ Polarization Data.

E_d (MeV)	θ_{lab} (deg)	$\theta_{C.M.}$ (deg)	Asymmetry	SPF	$\overline{P_2}$	Polarization
2.2	10	10.6	0.053 ± 0.088	1.03	0.77	0.070 ± 0.117
	20	21.1	0.033 ± 0.031	1.03	0.77	0.040 ± 0.048
	30	31.6	0.121 ± 0.038	1.03	0.77	0.162 ± 0.051
	40	42.1	0.148 ± 0.019	1.03	0.77	0.198 ± 0.026
	60	62.8	0.050 ± 0.060	1.03	0.75	0.068 ± 0.081
	80	83.2	-0.092 ± 0.044	1.02	0.72	-0.128 ± 0.061
	100	103.2	0.038 ± 0.054	1.02	0.72	0.054 ± 0.076
	120	122.8	-0.066 ± 0.044	1.01	0.69	-0.096 ± 0.064
2.6	10	10.6	0.099 ± 0.103	1.07	0.85	0.123 ± 0.128
	20	21.1	0.036 ± 0.072	1.07	0.86	0.045 ± 0.090
	30	31.6	0.116 ± 0.047	1.07	0.86	0.145 ± 0.059
	40	42.1	0.116 ± 0.040	1.07	0.85	0.146 ± 0.050
	60	62.9	0.082 ± 0.038	1.06	0.84	0.104 ± 0.048
	80	83.2	0.060 ± 0.042	1.05	0.82	0.077 ± 0.054
	100	103.2	0.003 ± 0.045	1.04	0.79	0.004 ± 0.059
	120	122.9	0.032 ± 0.063	1.03	0.77	0.043 ± 0.084
3.0	10	10.6	-0.214 ± 0.087	1.12	0.91	-0.265 ± 0.108
	20	21.1	-0.104 ± 0.044	1.12	0.91	-0.129 ± 0.055
	30	31.6	-0.195 ± 0.039	1.12	0.91	-0.242 ± 0.048
	40	42.1	-0.212 ± 0.035	1.12	0.91	-0.263 ± 0.043
	60	62.9	-0.014 ± 0.037	1.11	0.89	-0.017 ± 0.046
	80	83.3	0.167 ± 0.054	1.09	0.88	0.207 ± 0.067
	100	103.3	0.346 ± 0.045	1.08	0.87	0.433 ± 0.056
	120	122.9	0.210 ± 0.076	1.07	0.86	0.267 ± 0.096
3.3	10	10.6	-0.054 ± 0.034	1.15	0.93	-0.067 ± 0.042
	20	21.1	-0.027 ± 0.037	1.15	0.93	-0.033 ± 0.046
	30	31.7	-0.021 ± 0.029	1.15	0.93	-0.026 ± 0.036
	40	42.1	-0.017 ± 0.021	1.14	0.92	-0.021 ± 0.026
	60	62.9	0.028 ± 0.023	1.13	0.91	0.035 ± 0.029

Table 10. (continued)

E_d (MeV)	θ_{lab} (deg)	$\theta_{C.M.}$ (deg)	Asymmetry	SPF	$\overline{P_2}$	Polarization
3.6	10	10.6	-0.032 ± 0.056	1.18	0.94	-0.040 ± 0.069
	20	21.1	-0.154 ± 0.069	1.18	0.94	-0.191 ± 0.086
	30	31.7	-0.140 ± 0.027	1.18	0.94	-0.174 ± 0.034
	40	42.1	-0.124 ± 0.019	1.17	0.94	-0.154 ± 0.024
	60	62.9	-0.072 ± 0.039	1.16	0.94	-0.089 ± 0.048
	80	83.3	0.154 ± 0.040	1.15	0.94	0.191 ± 0.050
3.9	10	10.6	-0.072 ± 0.051	1.21	0.94	-0.087 ± 0.062
	20	21.1	-0.089 ± 0.044	1.21	0.94	-0.114 ± 0.056
	30	31.7	-0.162 ± 0.035	1.21	0.94	-0.208 ± 0.045
	40	42.1	-0.211 ± 0.040	1.20	0.94	-0.268 ± 0.051
	60	62.9	-0.197 ± 0.043	1.19	0.94	-0.246 ± 0.060
	80	83.3	0.062 ± 0.048	1.18	0.94	0.077 ± 0.060
2.0	20		0.141 ± 0.075	1.02	0.72	0.198 ± 0.105
2.4	20		0.032 ± 0.059	1.05	0.82	0.041 ± 0.076
2.8	20		-0.206 ± 0.067	1.09	0.88	-0.256 ± 0.083
2.9	20		-0.084 ± 0.032	1.11	0.89	-0.104 ± 0.040
3.2	20		-0.033 ± 0.034	1.13	0.92	-0.041 ± 0.042
3.5	20		-0.281 ± 0.049	1.17	0.94	-0.349 ± 0.061
3.8	20		-0.190 ± 0.033	1.20	0.94	-0.240 ± 0.046
3.85	20		-0.205 ± 0.042	1.20	0.94	-0.260 ± 0.053
2.0	40		-0.050 ± 0.045	1.02	0.71	-0.071 ± 0.064
2.1	40		0.194 ± 0.048	1.02	0.72	0.266 ± 0.066
2.2	40		0.096 ± 0.039	1.03	0.76	0.130 ± 0.053
2.3	40		0.272 ± 0.030	1.03	0.78	0.363 ± 0.040
2.4	40		0.041 ± 0.039	1.05	0.81	0.053 ± 0.051
2.5	40		0.096 ± 0.056	1.06	0.83	0.122 ± 0.071
2.7	40		-0.023 ± 0.034	1.08	0.87	-0.029 ± 0.042

Table 10. (continued)

E_d (MeV)	θ_{lab} (deg)	Asymmetry	SPF	$\overline{P_2}$	Polarization
2.8	40	-0.280 ± 0.041	1.09	0.88	-0.347 ± 0.051
2.9	40	-0.135 ± 0.024	1.11	0.89	-0.168 ± 0.030
3.1	40	-0.160 ± 0.022	1.12	0.91	-0.197 ± 0.027
3.2	40	-0.105 ± 0.022	1.13	0.92	-0.130 ± 0.027
3.4	40	-0.066 ± 0.020	1.16	0.94	-0.082 ± 0.025
3.5	40	-0.326 ± 0.024	1.17	0.94	-0.404 ± 0.030
3.7	40	-0.083 ± 0.031	1.19	0.94	-0.104 ± 0.039
3.8	40	-0.418 ± 0.029	1.20	0.94	-0.526 ± 0.037
3.85	40	-0.298 ± 0.027	1.20	0.94	-0.378 ± 0.034

Table 11. The $^{24}Mg(d,n_1)$ Polarization Data.

E_d (MeV)	θ_{lab} (deg)	$\theta_{C.M.}$ (deg)	Asymmetry	SPF	$\overline{P_2}$	Polarization
2.2	10	10.6	-0.001 ± 0.016	1.01	0.66	-0.002 ± 0.025
	20	21.3	-0.033 ± 0.010	1.01	0.65	-0.052 ± 0.016
	30	31.9	-0.118 ± 0.016	1.01	0.63	-0.188 ± 0.025
	40	42.4	-0.282 ± 0.010	1.00	0.62	-0.451 ± 0.019
	60	63.2	-0.181 ± 0.021	1.00	0.59	-0.304 ± 0.035
	80	83.7	-0.058 ± 0.013	1.00	0.58	-0.093 ± 0.021
	100	103.7	-0.072 ± 0.020	1.00	0.55	-0.131 ± 0.036
	120	123.2	-0.015 ± 0.027	1.00	0.54	-0.028 ± 0.050
2.6	10	10.6	-0.026 ± 0.017	1.03	0.77	-0.035 ± 0.023
	20	21.2	-0.073 ± 0.016	1.03	0.77	-0.099 ± 0.022
	30	31.8	-0.165 ± 0.023	1.03	0.75	-0.222 ± 0.031
	40	42.4	-0.290 ± 0.030	1.03	0.75	-0.392 ± 0.040
	60	63.2	-0.049 ± 0.023	1.02	0.73	-0.067 ± 0.032
	80	83.6	-0.040 ± 0.021	1.02	0.72	-0.057 ± 0.030
	100	103.6	-0.001 ± 0.028	1.01	0.69	-0.001 ± 0.041
	120	123.2	-0.078 ± 0.054	1.01	0.66	-0.120 ± 0.083
3.0	10	10.6	0.040 ± 0.014	1.07	0.86	0.050 ± 0.018
	20	21.2	-0.028 ± 0.016	1.07	0.86	-0.035 ± 0.020
	30	31.8	-0.170 ± 0.020	1.06	0.84	-0.214 ± 0.025
	40	42.3	-0.290 ± 0.030	1.06	0.84	-0.368 ± 0.038
	60	63.1	-0.060 ± 0.020	1.05	0.82	-0.077 ± 0.026
	80	83.6	-0.015 ± 0.026	1.04	0.79	-0.020 ± 0.034
	100	103.6	0.011 ± 0.027	1.03	0.77	0.015 ± 0.036
	120	123.1	0.036 ± 0.037	1.03	0.75	0.049 ± 0.050
3.3	10	10.6	-0.030 ± 0.008	1.10	0.81	-0.037 ± 0.010
	20	21.2	-0.061 ± 0.011	1.10	0.89	-0.076 ± 0.013
	30	31.8	-0.074 ± 0.034	1.09	0.88	-0.092 ± 0.042
	40	42.3	-0.098 ± 0.023	1.09	0.88	-0.122 ± 0.029
	60	63.1	0.224 ± 0.015	1.08	0.87	0.278 ± 0.019

Table 11. (continued)

E_d (MeV)	θ_{lab} (deg)	$\theta_{C.M.}$ (deg)	Asymmetry	SPF	$\overline{P_2}$	Polarization
3.6	10	10.6	-0.004 ± 0.008	1.13	0.92	-0.005 ± 0.010
	20	21.1	-0.008 ± 0.014	1.13	0.92	-0.010 ± 0.017
	30	31.8	0.090 ± 0.018	1.12	0.91	0.112 ± 0.022
	40	42.3	0.232 ± 0.019	1.12	0.91	0.288 ± 0.023
	60	63.1	0.133 ± 0.023	1.12	0.91	0.165 ± 0.029
	80	83.5	0.037 ± 0.031	1.11	0.89	0.046 ± 0.038
3.9	10	10.6	0.006 ± 0.010	1.17	0.94	0.007 ± 0.012
	20	21.2	0.000 ± 0.014	1.16	0.94	0.000 ± 0.017
	30	31.8	-0.008 ± 0.020	1.16	0.94	-0.010 ± 0.025
	40	42.3	-0.234 ± 0.039	1.16	0.94	-0.290 ± 0.048
	60	63.1	-0.225 ± 0.038	1.15	0.93	-0.278 ± 0.047
	80	83.5	-0.064 ± 0.025	1.12	0.91	-0.079 ± 0.031
2.0	20		-0.026 ± 0.009	1.00	0.58	-0.045 ± 0.016
2.4	20		0.003 ± 0.010	1.02	0.72	0.004 ± 0.014
2.8	20		-0.079 ± 0.010	1.05	0.82	-0.102 ± 0.013
2.9	20		-0.052 ± 0.009	1.06	0.84	-0.066 ± 0.011
3.2	20		-0.086 ± 0.008	1.09	0.88	-0.107 ± 0.010
3.5	20		-0.149 ± 0.012	1.12	0.91	-0.185 ± 0.015
3.8	20		0.082 ± 0.009	1.16	0.94	0.102 ± 0.011
3.85	20		-0.015 ± 0.011	1.16	0.94	-0.019 ± 0.014
2.0	40		-0.127 ± 0.012	1.00	0.54	-0.236 ± 0.021
2.1	40		-0.190 ± 0.023	1.00	0.58	-0.332 ± 0.040
2.2	40		-0.264 ± 0.021	1.00	0.61	-0.439 ± 0.035
2.3	40		-0.272 ± 0.013	1.01	0.66	-0.420 ± 0.020
2.4	40		-0.162 ± 0.017	1.01	0.69	-0.236 ± 0.025
2.5	40		-0.277 ± 0.021	1.02	0.72	-0.388 ± 0.029
2.7	40		-0.252 ± 0.024	1.03	0.77	-0.335 ± 0.032

Table 11 (continued)

E_d (MeV)	θ_{lab} (deg)	Asymmetry	SPF	$\overline{P_2}$	Polarization
2.8	40	-0.147 ± 0.023	1.04	0.79	-0.193 ± 0.030
2.9	40	-0.313 ± 0.023	1.05	0.82	-0.404 ± 0.030
3.1	40	-0.186 ± 0.022	1.07	0.86	-0.232 ± 0.027
3.2	40	-0.064 ± 0.027	1.08	0.87	-0.079 ± 0.034
3.4	40	0.033 ± 0.032	1.11	0.89	0.041 ± 0.040
3.5	40	0.085 ± 0.040	1.12	0.91	0.106 ± 0.050
3.7	40	0.151 ± 0.027	1.13	0.92	0.187 ± 0.034
3.8	40	-0.120 ± 0.031	1.15	0.93	-0.149 ± 0.029
3.85	40	-0.155 ± 0.030	1.15	0.93	-0.192 ± 0.037

Chapter VI

The $^{40}Ca(d,n_0)$ Neutron Polarization at 3.8 MeV

A. Introduction

The interaction of deuterons with ^{40}Ca has been the subject of several experiments and analyses. Recently Schwandt and Haeberli[22] have obtained optical model parameters which yield good agreement with the deuteron elastic scattering cross sections and polarization data. Their studies have provided one of the few determinations of the spin-orbit potential for deuteron scattering. DWBA calculations with these parameters fit the $^{40}Ca(d,p_0)$ cross section data but failed to describe adequately the proton polarization. It is of interest to see if the mirror reaction also presents this difficulty.

It was originally intended to study the $^{40}Ca(d,n_0)$ reaction at tandem Van de Graaff energies in order to have more information to test the DWBA predictions. The data presented here are the result of a preliminary study using the 4 MeV Van de Graaff accelerator to test the feasibility of using our present methods to measure the polarizations at higher energies.

This preliminary study indicated that an accurate measurement at tandem energies would take prohibitively long with our present techniques. One would have to have an exceptionally good helium cell and use small side detector scintillators (hence low counting rate) in order to separate the $^{40}Ca(d,n)$ neutrons from contaminant neutrons.

B. Experiment

Targets for these measurements were prepared by evaporating natural calcium metal from an Al_2O_3 crucible onto tantalum endcaps. Since calcium forms $Ca(OH)_2$ readily upon contact with moist air and since oxygen is a serious contaminant, appreciable care must be taken to keep oxidation to a minimum. The targets were therefore sealed against a glass plate with an O-ring before they were removed from the vacuum. The beam pipe was let up to atmospheric pressure with dry nitrogen before the target was transferred so that the target was exposed to the air only momentarily. Even so, some oxygen contamination was found to be inevitable. The targets had a thickness which corresponded to an energy loss of about 200 keV in the incident beam. The thickness was determined by weighing a small square of tantalum which was positioned beside the endcap during the evaporation. The mean deuteron energy in the target was 3.8 MeV. The side detectors were NE-213 liquid organic scintillators (5.08 cm by 7.62 cm by 15.3 cm) which were mounted at 120° (lab) 23 cm (center to center) from the helium cell.

The solenoid was operated at currents that precessed the spins of the $^{40}Ca(d,n_0)$ neutrons by 90°. Figure 20 shows one of the better coincidence gated recoil spectra.

C. Results and Comparison with Other Data

Table 12 gives the results of the measurements. The data are compared in Fig. 20 to the DWBA calculations using non-local, finite range approximation of the computer code DWUCK of P. D. Kunz.[22] The reaction is represented by a proton transfer to the $f_{7/2}$ shell in ^{41}Sc. Also shown in the figure are the 6 MeV data of Gedcke et al.[52] and the 4 MeV cross section data of Macefield, Towle and Gilboy.[53] Table 13 gives the deuteron optical model parameters for each of the curves in Fig. 19. Potential set D1 at 6 MeV is from Schwandt and Haeberli[51] and the other two sets at this energy are modifications of this set. At 3.8 MeV, the calculations were made using parameters centered around extrapolated values of Schwandt and Haeberli. In all these calculations the neutron parameters were held fixed. They originated with Perey and Buck and are taken from Ref. 52. The largest sensitivity in the DWBA results at 3.8 MeV was observed when the real well radius r_0 was increased by several percent. (Because of the Vr_0^n ambiguity this corresponds to the effect seen when V is deepened.) This sensitivity is demonstrated by comparing the curves for potential D6 to those for D7. The sensitivity to changes in W' and V_{so} are also displayed. Calcu-

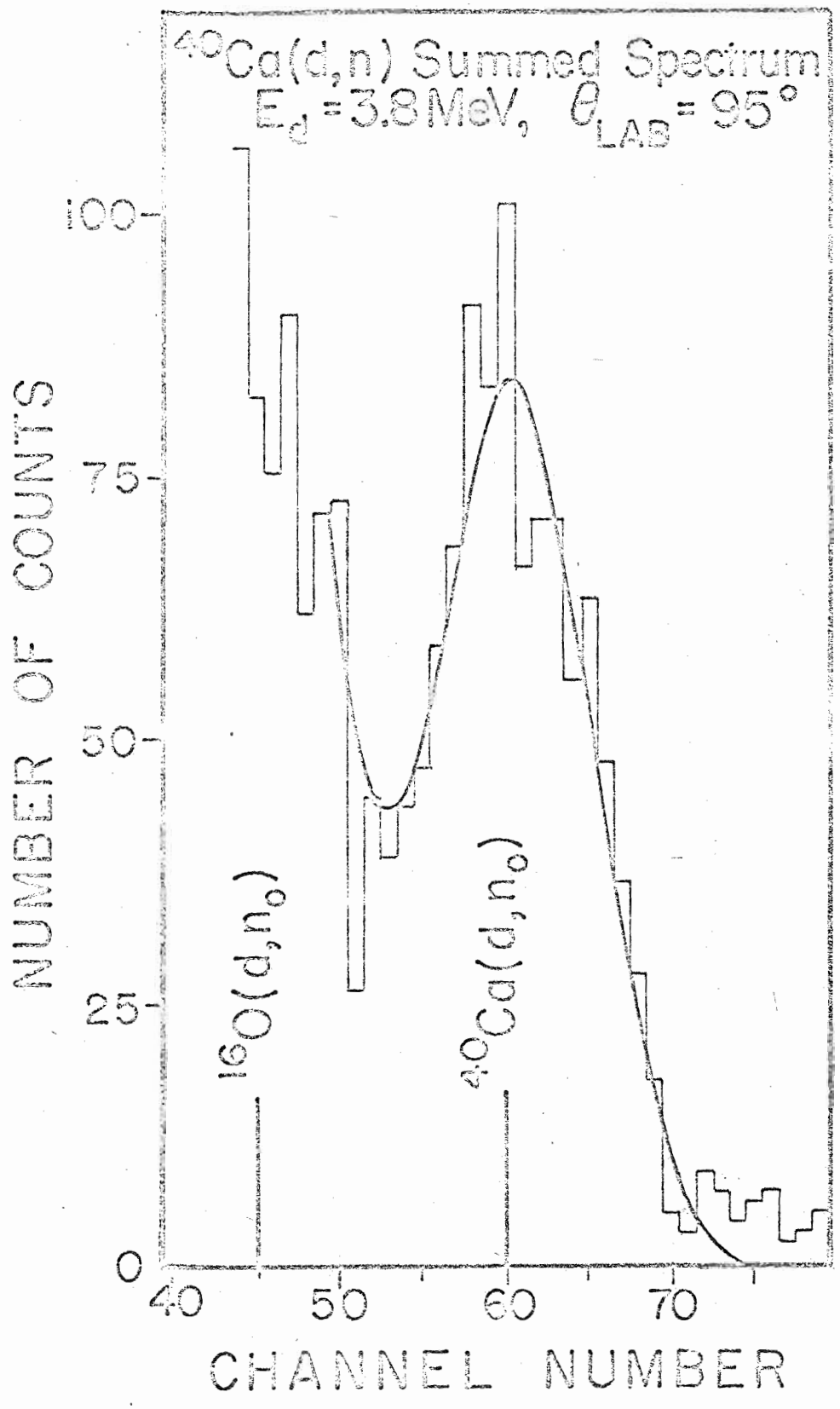

Figure 20. Summed Spectrum for ^{40}Ca(d,n).

Table 12. The $^{40}Ca(d,n_0)$ Polarization at 3.8 MeV.

θ_{lab} (deg)	$\theta_{C.M.}$ (deg)	Asymmetry	$\overline{P_2}$	Polarization
20.0	20.8	-0.148 ± 0.058	0.87	-0.17 ± 0.07
35.0	36.4	-0.043 ± 0.071	0.87	-0.05 ± 0.08
45.0	46.8	0.017 ± 0.037	0.87	0.02 ± 0.04
57.5	59.5	0.008 ± 0.036	0.87	0.01 ± 0.04
65.0	67.2	0.040 ± 0.044	0.87	0.05 ± 0.05
80.0	82.4	-0.012 ± 0.052	0.87	-0.01 ± 0.06
95.0	07.4	0.016 ± 0.042	0.87	0.02 ± 0.05
110.0	112.3	-0.039 ± 0.052	0.87	-0.04 ± 0.06

Table 13. Deuteron Optical Model Potential Sets.

Energy (MeV)	Potential	V (MeV)	r_o (fm)	a_o (fm)	W (MeV)	r_i (fm)	a_i (fm)	V_{so} (MeV)	r_{so} (fm)	a_{so} (fm)
6.0	D1	115.5	1.05	0.85	9.5	1.65	0.52	9.0	0.9	0.60
6.0	D2	115.5	1.05	0.85	9.5	1.65	0.52	0.0	0.9	0.60
6.0	D3	115.5	1.075	0.85	8.0	1.65	0.52	9.0	0.9	0.60
3.8	D4	112.0	1.075	0.80	8.5	1.67	0.51	9.0	0.9	0.52
3.8	D5	112.0	1.075	0.80	9.0	1.67	0.51	8.5	0.9	0.52
3.8	D6	112.0	1.075	0.80	7.0	1.67	0.51	0.0	0.9	0.52
3.8	D7	112.0	1.05	0.80	8.5	1.67	0.51	0.0	0.9	0.52

Key for Fig. 21

D1 ———

D2 — • — • —

D3 — — —

D4 ———

D5 — — —

D6 • • • • •

D7 • — • — •

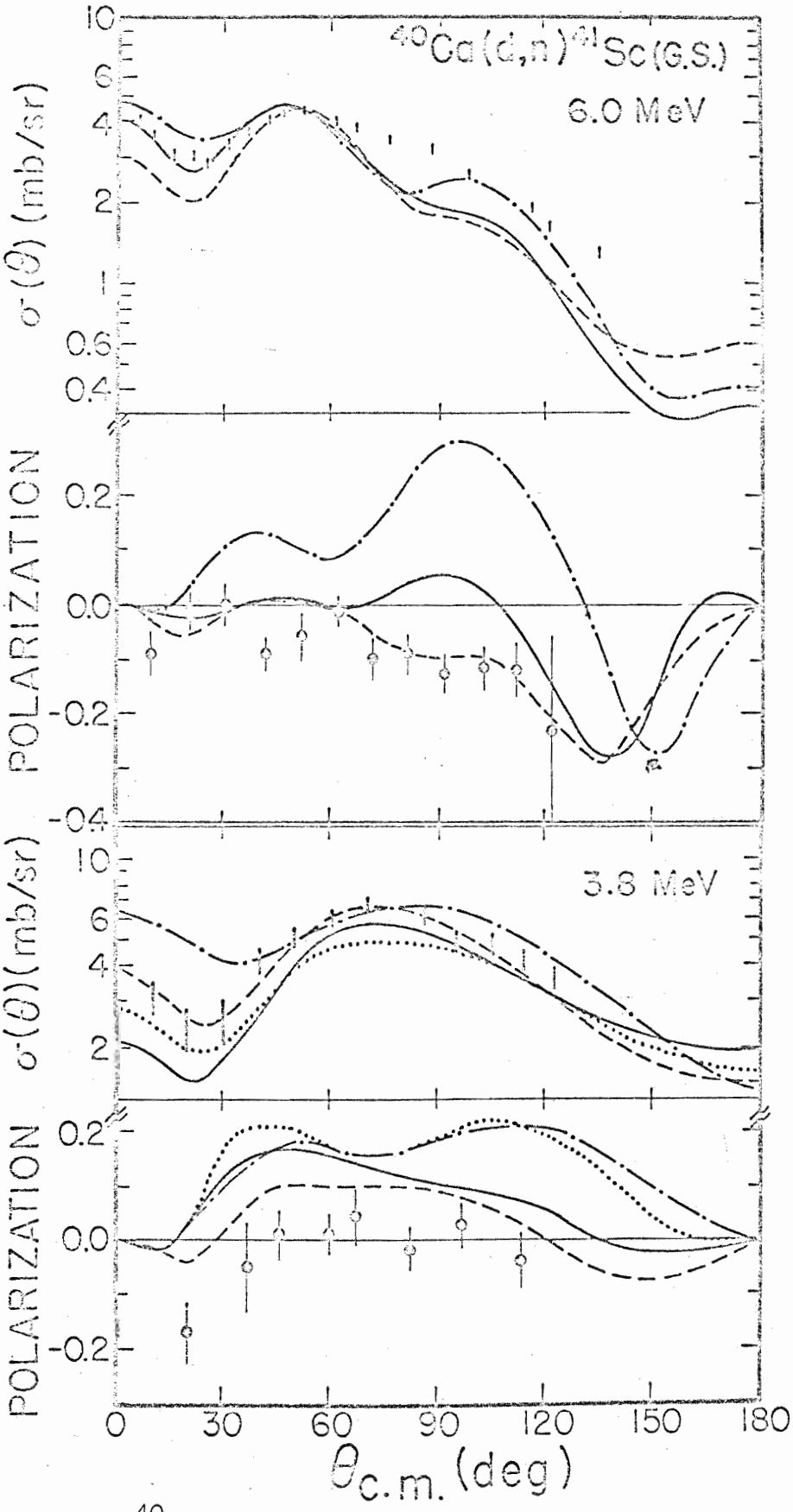

Figure 21. ^{40}Ca(d,n) Cross Section and Polarization Data Compared with DWBA Calculations. Displayed in addition to the present polarization data at 3.8 MeV are data from Refs. 52, 53, and 51

lations have been made at 5 MeV where $^{40}Ca(d,p)$ cross section and polarization data exist and it was found that the above parameter changes do not affect the shape of the calculated cross section but do help the polarization agreement somewhat. It seems that DWBA calculations may yield suitable fits if appreciable parameter searching were undertaken, but until more is known about deuteron D-state effects and the effect of coupling in other channels,[25] further trimming of the parameters has questionable value.

Chapter VII

CONCLUSION

The stripping reactions studied in this thesis exhibit a wide variety of polarization patterns. It is clear from those reactions where data are available over a wide range of energies that any generalizations of these reactions solely on the shapes of their polarization distributions will meet with little success. For instance, the empirical rule of Reber and Saladin[10] and Meier et al.[9] on the differences in $p_{1/2}$ and $p_{3/2}$ stripping polarization distributions does not hold for the $^{11}B(d,n)$ reactions. Moreover, these distributions change significantly with a few MeV change in deuteron energy.

The DWBA calculations give only modest agreement for the $^{11}B(d,n_0)$ reaction and poor agreement for the $^{11}B(d,n_1)$ reaction. There are two points which should be mentioned about the ^{11}B analysis. Firstly, the optical model analysis was performed at only three energies with scattering data taken with thin targets. The parameters obtained did not have a smooth energy dependence. This was probably caused by insufficient averaging of compound nucleus effects and might be alleviated by using thicker targets. Secondly, the DWBA results obtained by damping the wave

functions in the nuclear interior were encouraging. These results tend to indicate that a more sophisticated approach might be appropriate. The wave functions in this region are not well determined by the optical model analysis, but they give a large contribution to the (d,n) cross section and polarization.

The DWBA calculations describe the $^{28}Si(d,n_0)$ reaction comparatively well. The calculations for $^{28}Si(d,n_1)$ fit the cross sections fairly well also, but the polarization misses badly. These results for $^{28}Si(d,n)$ are particularly interesting. The good results for the n_0 reaction would imply that either the n_0 reaction is grossly insensitive to the details of the calculations or else the poor results for the n_1 reaction is indicative of a major failing of the model. It seems to be more than just the usual difficulties of poor optical model parameters or strong compound nucleus contributions.

The polarization of $^{24}Mg(d,n_0)$ and $^{24}Mg(d,n_1)$ showed sizeable compound nucleus effects so no DWBA comparisons were made. The results for $^{40}Ca(d,n_0)$ are inconclusive but indicate moderate success may be possible, particularly at 6 MeV.

Descriptions using the DWBA model were plagued with inconsistencies. The success of the DWBA for some reactions is offset by the fact that one must be extremely cautious before drawing conclusions about (d,n) reactions on targets lighter than ^{40}Ca. Perhaps the inclusion of corrections such as tensor forces, the deuteron D state, and the effects of coupling in other channels would improve the results. Other reaction models may very

well turn out to be more accurate than the DWBA but this remains to be demonstrated. The large amount of polarization data being accumulated, including the polarized source measurements, should provide stringent tests of these models.

Appendix A

THE COMPUTER CODE ASP

A. Purpose

The program ASP is a computer code designed for extracting asymmetry information from coincidence-gated recoil spectra. The gated recoil spectra are described as a sum of Gaussian peaks and a linear or quadratic background. The program can automatically optimize the amplitudes of these peaks, or the operator may choose to adjust them manually. The program operates on the DDP-224 computer and requires floating point hardware and a display tube. It uses less than 8K words of core storage and can fit up to 4 neutron groups simultaneously. It can also fit the quadratic background with up to three of the peaks if there is enough information in the spectra for it to do a reasonable job.

B. Method of Fitting

The spectra which are input to the program are a Left spectrum and a Right spectrum as defined in Chapter II. These spectra are normally

generated from the original spectra by the program NPOL of R. A. Hardekopf.[53] Also generated is a spectrum calculated from the backgrounds which are used to correct the original spectra. This spectrum is used to provide the correct weighting factors for the optimization since the corrected spectrum does not carry the statistical error associated with each channel. As long as the backgrounds are small this makes little difference. The effect can be important in the case of gas targets where large "gas out" backgrounds are subtracted, especially in the estimation of the statistical error associated with the asymmetry. This method of background correction is equivalent to fitting an uncorrected spectrum with a spectrum composed of the calculated spectrum and the backgrounds.

Since the calculated spectra are described by a linear superposition of the parameters which are to be fitted, the problem reduces to solving a set of linear equations. The function which is minimized is the χ^2, which is defined as

$$\chi^2 = \sum_i \frac{(N_i - F_i)^2}{W_i^2}$$

Here N_i stands for the piece of the experimental spectrum which is being fitted and F_i is the corresponding calculated spectrum. The variable W_i is the statistical weight of each point. In the present case the spectrum to be fitted is a section of the Left spectrum appended to the corresponding piece of the Right spectrum. The two pieces are fitted simultaneously because they are often coupled by a background which is taken to be unpolarized

or else a constant asymmetry recoil peak. The following procedure to minimize the χ^2 and hence fit the spectra is similar to that of Bevington.[54] The calculated spectrum is written as

$$F_i = \sum_j a_j f_{ij} \ ,$$

where f_{ij} is usually a normalized Gaussian (unit area) with resolution (relative FWHM) of $(ARES + BRES/E)^{1/2}$. Here E is the neutron energy. The function f_{ij} may also be one of the terms of the quadratic background. Since χ^2 is to be minimized, the procedure is to set

$$\frac{\partial \chi^2}{\partial a_i} = 0$$

for j = 1 to NTERMS. The variable NTERMS is the total number of functions in the fit. Then

$$\sum_j a_j \sum_i \frac{1}{w_i^2} f_{ij} f_{ik} = \sum_i \frac{N_i}{w_i^2} f_{ik} \quad \text{for K=1 to NTERMS.}$$

Defining

$$C_{jk} = \sum_i \frac{1}{w_i^2} f_{ij} f_{ik}$$

and

$$B_k = \sum_i \frac{N_i}{w_i^2} f_{ik} \ ,$$

the equations can be written in matrix notation as

$$C \cdot A = B \ .$$

The vector A represents the amplitudes a_j. The problem is easily solved by inverting the matrix C. The subroutine MATINV of Bevington[54] is used to

accomplish this task. The diagonal elements C_{jj}^{-1} of the inverted matrix are the square of the errors associated with each of the amplitudes A_j.

C. Program Operation

Typewriter Input:

KEVCxxxx	The number xxxx is the kilovolts/channel and can be adjusted with a sense switch operation.
ENRGbbbbb xxxxxxxx	The incident energy in keV is xxxx. The notation b denotes a blank.
ANGLxxxx	The laboratory angle in degrees is xxxx.
ARESxxxx	The resolution parameter ARES is .0001*xxxx.
BRESxxxx	The resolution parameter BRES is 0.0001*xxxx. The relative FWHM for a neutron group is $(ARES+BRES/EN)^{1/2}$, where EN is the neutron energy in MeV.
+ASMbbbbk bbbbxxxx	The asymmetry of group k is set to 0.0001*xxxx.
-ASMbbbbk bbbbxxxx	The asymmetry of group k is set to -0.0001*xxxx. The instructions +ASM and -ASM cause the asymmetry to be fixed only when IA(k) is 2 or 3 as will be described later.

RATOØØØk ØØØjxxxx — The sum of group k is held to 0.1*xxxx times the sum of group j. This is not active unless IA(k) is 3. This option requires that a constant asymmetry be input for group k.

DELExxxx — The incident particle energy is always decreased by xxxx (in keV) before calculating the neutron energies. This is to compensate for the target thickness.

ZEROØØØk — The Left and Right amplitudes for group k are set to zero and the entire search is turned off by setting the IA array and the quadratic background search flag to zero.

Sense Switch Operations:

Switches 1-5. These switches set the IA array which controls the fitting in the following way. The variable IFLAG is set to either 0, 1, 2, 3, or 5 by the particular switch chosen. The value is then transferred to IA(K) by light penning the vertical line at the position of the Kth group. The IA array has the following interpretation:

IA(K) = 0 means group K will not be affected by the fitting procedure.

IA(K) = 1 means the Left and Right amplitudes will be fit.

IA(K) = 2 means fit on group K but hold its asymmetry fixed to the value input by typewriter.

IA(K) = 3 means the sum of group K will be held to RATO(K)*(AL(IRAT(K)) + AR(IRAT(K)) and keep the asymmetry constant. These numbers are input by the typewriter instructions RATO, +ASM, and -ASM.

IA(K) = 5 means do not change the IA array if a light pen interrupt is received.

Switch 6. Adjust the variables ARES and BRES with the Horizontal and Vertical switches. Adjustment is terminated when the word "END?" is light penned on the display scope.

Switch 7. Adjust the energy scale with the Horizontal and Vertical switches in the same manner as switch 6.

Switch 8. Adjust the background. The quadratic background search flag must be off. The linear background is adjusted with the Horizontal and Vertical switches. The Horizontal switch controls the slope and the Vertical switch increases or decreases the y-intercept.

Switch 9. Read the kinematics cards. One card is required for each group. They must be followed by a blank card. No more than 5 groups are allowed. Input is zero

padded I8 format the incident particle mass times 1000 (in AMU), the target mass times 1000 (in AMU), and the Q value (in keV). For negative Q values the first two characters of its field should be "Ø-" .

$^{40}Ca(d,n)$ Q = -1.14 MeV:

0000200000040000 -001140

$^{28}Si(d,n)$ Q = 0.528 MeV:

000020000002800000000528

Switch 10. Initialize the linear background and go to switch 8. The slope is set to zero and the y intercept is set to a value proportional to the Range switch setting.

Switch 11. Adjust the Left and Right amplitudes of each of the neutron groups using the Horizontal and Vertical switches. A question mark is displayed above the peak of the group being adjusted. When the question mark is light penned the adjustment procedure moves to the next group. The procedure is terminated by light penning the word "END?" on the display screen. The Vertical switch controls the Left amplitudes and the Left spectrum is displayed above the Right one.

Switch 12. Initializes all of the peak amplitudes to 2 times the value of the Range switch.

Switch 13. Outputs the asymmetry and amplitude information on the typewriter.

Switch 14. Calculates the asymmetry between the light penned channels by summing the spectra and displays the results on the screen. If the word "YES" is light penned the line of information is typed out. If "NO" is light penned the program reverts to its normal display loop. The IA array should be zero before this operation is done. The program calculates the spectra with the amplitudes that it has and uses these spectra as a background. A statistical uncertainty of the square root of the number of counts is assigned to these spectra during the calculations.

Switch 15. Fits the spectra between the light penned channels following the directions of the IA array.

Switch 16. Reads the Left and Right spectra from paper tape. Also reads the energy, angle and the spectrum composed of the backgrounds. The paper tape is generated with the program NPOL of Hardekopf.[53]

Switch 17. Turns the quadratic background search flag on.

Switch 18. Turns the quadratic background search flag off.

Appendix B

The $^{11}B(d,d)$ Elastic Scattering Data of R. A. Hardekopf, J. Taylor, and R. L. Walter *

$\theta_{C.M.}$ (deg)	7.5 MeV σ/σ_R		9.5 MeV σ/σ_R	
17.73	1.21	± 0.02	1.49	± 0.02
23.60	1.54	± 0.03	1.96	± 0.03
29.45	1.73	± 0.03	2.15	± 0.04
35.27	1.59	± 0.03	1.56	± 0.03
41.05	1.04	± 0.02	0.65	± 0.01
46.78	0.43	± 0.00	0.17	± 0.00
52.46	0.35	± 0.00	0.52	± 0.01
58.09	0.83	± 0.01	1.47	± 0.02
63.65	1.78	± 0.03	2.78	± 0.05
69.15	2.96	± 0.05	3.42	± 0.06
74.58	3.74	± 0.07	3.55	± 0.07
79.94	3.90	± 0.07	3.61	± 0.07
85.22	3.86	± 0.07	3.44	± 0.06
90.42	3.85	± 0.07	2.71	± 0.05
95.54	3.56	± 0.07	2.70	± 0.05
100.58	2.43	± 0.04	2.93	± 0.05
105.54	2.33	± 0.04	3.12	± 0.06
110.40	2.81	± 0.05	3.85	± 0.07
115.21	3.83	± 0.07	4.51	± 0.09
119.93	4.99	± 0.09	4.94	± 0.09
124.57	6.48	± 0.12	6.65	± 0.13

$\theta_{C.M.}$ (deg)	7.5 MeV σ/σ_R		9.5 MeV σ/σ_R	
129.15	7.94	± 0.15	8.64	± 0.17
133.65	9.63	± 0.19	11.23	± 0.22
138.08	11.37	± 0.22	13.89	± 0.27
142.46	12.69	± 0.25	17.06	± 0.34
146.77	12.84	± 0.25	19.79	± 0.39
151.04	13.52	± 0.27	21.72	± 0.43
155.26	14.53	± 0.29	23.69	± 0.47
159.45	15.72	± 0.31	24.67	± 0.49
163.60	16.13	± 0.32	24.92	± 0.49
167.72	16.18	± 0.32	24.89	± 0.49

* Errors quoted are statistical only. Absolute normalization is ± 15%.

LIST OF REFERENCES

LIST OF REFERENCES

1. P. J. Bjorkholm, W. Haeberli, and B. Mayer, Phys. Rev. Lett. 22, 955 (1969).

2. G. L. Morgan and R. L. Walter, Nucl. Instr. Methods 58, 227 (1968).

3. N. R. Roberson, R. V. Poore, F. Seibel, and J. Joyce in Proceedings for the Skytop Conference on Computer Systems in Nuclear Physics, Skytop, Pa., 1969 (Columbia University Press, New Yor, 1969).

4. R. S. Thomason (unpublished Ph. D. Dissertation, Duke University, 1969).

5. D. Sukis (unpublished M. S. Thesis, The Ohio State University, 1966).

6. Th. Stammbach, J. Taylor, G. Spalek, and R. L. Walter, Phys. Rev. (3) 2, 434 (1970).

7. M. M. Meier, (unpublished Ph. D. Dissertation, Duke University, 1969).

8. S. Cohen and D. Kurath, Nucl. Phys. A101, 1 (1967).

9. M. M. Meier, F. O. Purser, G. L. Morgan and R. L. Walter, Symposium on Nuclear Mechanisms and Polarization Phenomena (Universite' Laval, Quebec, 1969).

10. L. H. Reber and J. X. Saladin, Phys. Rev. 133, B1155 (1964).

11. M. M. Meier, R. L. Walter, T. R. Donoghue, R. G. Seyler, and R. M. Drisko, Nucl. Phys. (in press).

12. D. H. Wilkinson, Phil. Mag. 3, 1185 (1958).

13. G. R. Satchler, L. W. Owen, A. J. Elwyn, G. L. Morgan, and R. L. Walter, Nucl. Phys. A112, 1 (1968).

14. B. Hoop and H. H. Barschall, Nucl. Phys. 83, 65 (1966).

15. W. Busse, B. Efken, D. Hilscher, J. A. Scheer and W. Wenning, Nucl. Phys. A152, 354 (1970).

16. V. A. Smotryaev and I. S. Trostin, JETP (Sov. Phys.) 19, 1012 (1964).

17. P. R. Almond and J. R. Risser, Nucl. Phys. 72, 436 (1965).

18. Th. Stammbach (private communication).

19. W. Fitz, R. Jahr, and R. Santo, Nucl. Phys. A101, 449 (1967).

20. R. A. Hardekopf (to be published).

21. W. J. Thompson (private communication).

22. P. Schwandt and W. Haeberli, Nucl. Phys. A123, 401 (1969).

23. P. D. Kunz (unpublished).

24. B. A. Watson, P. P. Singh, and R. E. Segel, Phys. Rev. 182, 977 (1969).

25. G. H. Rawitscher and S. N. Mukherjee, Phys. Rev. 181, 1518 (1969).

26. F. Machali, Atomkernenergie 13, 29 (1958).

27. H. Lacek and U. Strohbusch, Z. Physik 233, 101 (1970).

28. D. P. Gurd, G. Roy, and H. G. Leighton, Nucl. Phys. A120, 94 (1968).

29. P. Schwandt and W. Haeberli, Nucl. Phys. A110, 585 (1968).

30. W. Lorenz, C. Mayer-Boricke, R. Santo, and U. Schmidt-Rohr, Nucl. Phys. 46, 25 (1962).

31. S. G. Demortier and P. C. Macq, J. Phys. Radium 22, 597 (1961).

32. Y. V. Gofman and O. F. Nemets, JETP (Sov. Phys.) 13, 333 (1961).

33. H. Niewodniczanski, J. Nurzynski, A. Strzalkowski, J. Wilczynski, J. R. Rook, and P.E. Hodgson, Nucl. Phys. 55, 386 (1964).

34. B. H. Wildenthal, R. W. Krone, and F. W. Prosser, Phys. Rev. 135, B680 (1964).

35. U. Strohbusch, W. Bakowsky, and H. Lacek, Nucl. Phys. A149, 605 (1970).

36. J. A. Kuehner, E. Almqvist, and D. A. Bromley, Nucl. Phys. 21, 555 (1960).

37. J. R. Holt and T. N. Marsham, Proc. Phys. Soc. (London) A66, 467 (1953).

38. N. I. Zaika, Ukr. Fiz. Zh. 8, 492 (1963).

39. A. Isoya and M. J. Marrone, Phys. Rev. 128, 800 (1962).

40. R. W. Bercaw and F. B. Shull, Phys. Rev. 133, B632 (1964).

41. W. E. Maddox, C. T. Kelley, Jr., and D. W. Miller, Phys. Rev. (3) 1, 476 (1970).

42. M. V. Pasechnik, L. S. Saltykov, and D. I. Tambovtsev, JETP (Sov. Phys.) 16, 1111 (1963).

43. R. Felst, M. Cosack, T. Gudehus, R. H. Siemssen, J. Tepel, and B. Zeitnitz, Nucl. Phys. A108, 666 (1968).

44. W. G. Davies, W. K. Dawson, G. C. Neilson, and K. Ramavataram, Nucl. Phys. 76, 65 (1966).

45. S. G. Buccino, D. S. Gemmel, L. L. Lee, Jr., J. P. Schiffer, and A. B. Smith, Nucl. Phys. 86, 353 (1966).

46. J. M. Calvert, A. A. Jaffe, and E. E. Maslin, Proc. Phys. Soc. A70, 78 (1957).

47. S. T. Lam, D. A. Gedcke, G. M. Stinson, S. M. Tang, and J. T. Sample, Nucl. Phys. A119, 146 (1968).

48. F. G. Perey, Phys. Rev. 131, 745 (1963).

49. R. N. Glower, Phys. Lett. 16, 147 (1965).

50. O. Dietzsch, D. Wilmore, and P. E. Hodgson, Nucl. Phys. A106, 527 (1968).

51. D. A. Gedcke, S. T. Lam, S. M. Tang, G. M. Stinson, J. T. Sample, T. B. Grandy, W. J. McDonald, W. K. Dawson, and G. C. Neilson, Nucl. Phys. A134, 141 (1969).

52. B. E. F. Macefield, J. H. Towle, and W. B. Gilboy, Proc. Phys. Soc. 77, 1050 (1961).

53. R. A. Hardekopf (private communication).

54. P. R. Bevington, Data Reduction and Error Analysis for the Physical Sciences, McGraw-Hill, New York, N. Y., 1969, pp. 164-176.

BIOGRAPHY

John Taylor

Born: March 12, 1945
Columbia, South Carolina

Education: B.S. University of South Carolina, 1965
NDEA Fellow, 1965-1968
Research Assistant, 1968-1970

Publications:

Polarization in n-d Scattering at 7.8 MeV (with Spalek, Stammbach, Hardekopf, and Walter), Phys. Rev. (3) 1, 803 (1970).

The Polarization of Neutrons from the $^{40}Ca(d,n)^{41}Sc$ (G.S.) Reaction at 3.8 MeV (with Spalek, Stammbach, and Walter) (in press).

Neutron Polarization in the ($^{3}He,n$) Reactions on ^{11}B and ^{12}C (with Thomason, Stammbach, and Walter) (in press).

Determination of the Neutron Polarization from the $^{13}C(^{3}He,n)^{15}O$ (g.s.) Reaction from 2.9 to 3.9 MeV (with Stammbach, Thomason, and Walter), Phys. Rev. 174, 1119 (1968).

$^{9}Be(\alpha,n)$ as a Source of Polarized 7.8 MeV Neutrons (with Stammbach, Spalek, and Walter, Nucl. Inst. Meth. 80, 304 (1970).

Scattering of 7.8 MeV Polarized Neutrons from ^{4}He and the Phase Shifts Below 8 MeV (with Stammbach, Spalek, and Walter), Phys. Rev. (3) 2, 434 (1970).

Polarization of Neutrons from the $D(d,n)^3He$ Reaction from 6 to 14 MeV (with Spalek, Hardekopf, Stammbach, and Walter), Proceedings of the 3rd International Polarization Symposium, eds. H. H. Barschall and W. Haeberli, Madison, Wisconsin (1970) (to be published).

Cross Section and Polarization Measurements for the $^{11}B(d,n_0)$ and $^{11}B(d,n_1)$ Reactions (with Stammbach, Hardekopf, Spalek, and Walter, ibid.

Polarization Produced in the $^9Be(d,n)$ Reactions at 3.0 and 3.5 MeV and a Comparison to DWBA Calculations (with Spalek, Stammbach, Hardekopf, and Walter) ibid.

Abstracts:

Polarization of Neutrons from the $^9Be(d,n)^{10}B$ Reaction at 3.0 and 3.5 MeV (with Spalek, Stammbach, Hardekopf, and Walter), Bull. Am. Phys. Soc. 15, 482 (1970).

Neutron Polarization Distributions from the $^{11}B(d,n_0)$ and $^{11}B(d,n_1)$ Reactions at 7.5 and 9.5 MeV (with Stammbach, Hardekopf, Spalek, and Walter), Bull. Am. Phys. Soc. 15, 483 (1970).